TABLE OF CONTENTS

LIST OF FIGURES

LIST OF TABLES

LIST OF ABBREVIATIONS

ADP	adenosine di-phosphate
ATP	adenosine tri-phosphate
APN	aminopeptidase N
BB	brush border
DiD	1,1'-dioctadecyl-3,3,3',3'-tetramethylindodicarbocyanine perchlorate
DPPIV	Dipeptidyl-peptidase IV
EDTA	ethylene- di-amine tetra-acetic acid
EGTA	ethylene glycol tetra-acetic acid
FAVS	Fluorescence Activated Vesicle Sorting
FRAP	Fluorescence Recovery After Photobleaching
IAP	intestinal alkaline phosphatase
KO	knock out
LPH	lactase phlorizin hydrolase
LPS	lipopolysaccharide
LV	lumenal vesicle
MGAM	maltase glucoamylase
MSA	membrane shedding assay
MV	microvillus
myo1a	myosin-1a
myo2	myosin-2
Pi	inorganic phosphate

PIP_2	phosphatidylinositol bisphosphate
PI-PLC	phosphatidylinositol-specific phospholipase C
PLCδ	phospholipase C delta
PPi	pyrophosphate, $P_20_7^{4-}$
SEM	scanning electron microscopy
SI	sucrase-isomaltase
TEM	transmission electron microscopy
WT	wild type

CHAPTER I

INTRODUCTION

The intestinal epithelial cell

To obtain the energy and nutrients necessary for the maintenance of life, multi-cellular eukaryotes have evolved digestive tracts that store food internally while it is digested. Although internally located, the lumen of the digestive tract is necessarily open to the external environment to allow the entry of food; at the same time however, this access also allows this space to be colonized by large numbers of microbes. The incredibly large population (~10^{14}) of commensal bacteria that normally reside in the gut provide the host with a buffer against infection by pathogenic bacterial species and offer additional metabolic functionality (Backhed et al., 2005), such as the ability to digest some types of starch (Hooper and Gordon, 2001). A challenge posed by this arrangement is that the mucosal epithelial cells (enterocytes) must co-exist in intimate contact with lumenal microbes without succumbing to the toxic compounds and metabolites that are normally associated with bacterial populations. One such compound that is present at high levels in the intestinal lumen is the gram-negative bacterial outer membrane component, lipopolysaccharide (LPS, also known as “endotoxin”). LPS is a potent pro-inflammatory compound released from microbes as a soluble factor during cell division, growth, and death (Magalhaes et al., 2007). Toxic compounds and microbes are confined to the

lumen by a monolayer of epithelial cells joined at their apical surface by tight junctions (Fig. 1-1). In addition to acting as a physical barrier, it was recently shown that enterocytes help maintain the mucosal barrier by detoxifying LPS through the activity of intestinal alkaline phosphatase (IAP) (Bates et al., 2007). Both the physical and enzymatic barrier functions are carried out at the enterocyte apical surface by a specialized structure called the Brush Border (BB; Fig. 1-1).

The enterocyte brush border

Within the intestine, the BB functions as a barrier to the lumenal microbiota while simultaneously acting to process and absorb nutrients. Proper maintenance of the BB is vital to gut homeostasis: disruption of BB structure is associated with diseases such as microvillus inclusion disease (Cutz et al., 1989), a number of gluten-sensitive enteropathies (Bailey et al., 1989; Iancu and Elian, 1976), and is one of the first steps in the pathogenesis of adherent and invasive bacteria in the gut (Rolhion and Darfeuille-Michaud, 2007). In addition to serving as a physical barrier to microbe entry, BBs also possess enzymes that chemically modify bacterial compounds that would otherwise pose a threat to the mucosa. A critical part of this defense is the GPI-linked integral membrane protein, intestinal alkaline phosphatase (IAP), which has been shown to detoxify LPS by dephosphorylating the lipid A moiety (Poelstra et al., 1997). Recent studies in germ-free zebrafish have shown that mucosal IAP expression is induced in response to lumenal LPS and is critical for protecting animals from LPS toxicity (Bates et al., 2007). Moreover, mice lacking IAP demonstrate a reduced ability to

prevent bacterial translocation across the mucosal barrier following ischemic injury (Goldberg et al., 2008). An intriguing finding of the latter study is that high levels of IAP activity are present in the lumen of both the small and large bowel, although it is not known how IAP is released from the BB into the intestinal lumen. Despite the obvious physiological importance of the BB, the molecular functions of many of its key components remain unknown.

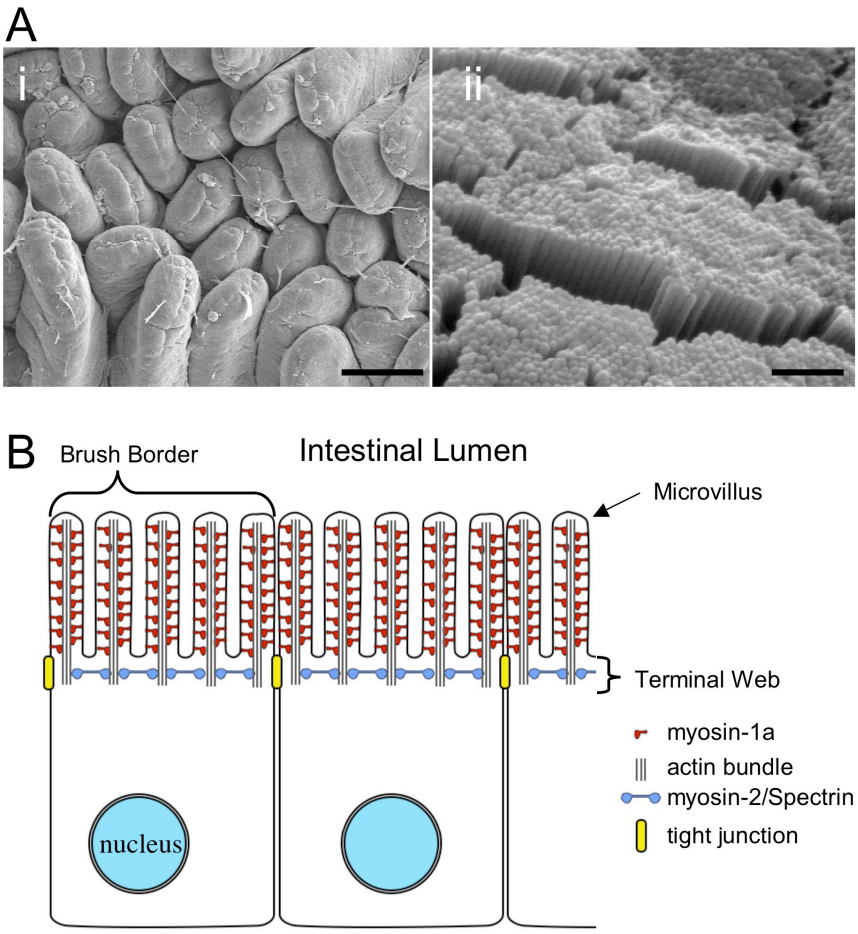

Fig. 1-1. Overview of intestinal brush border structure.
(A) SEM micrographs of the intestinal epithelium. (i) Low magnification view showing the finger-like projections called villi that protrude into the intestinal lumen. Each villus is covered by a monolayer of epithelial cells called enterocytes; the apical domain of enterocytes, called the brush border, faces the intestinal lumen and is composed of a hexagonal array of microvilli, seen in higher magnification in (ii). **(B)** Diagram of enterocyte organization. Neighboring enterocytes are held together by tight junctions, such that the only surface exposed to the intestinal lumen is the outer face of the microvillar membrane. Each microvillus is mechanically supported by a core actin bundle, and is linked to the overlying apical membrane by an array of myosin-1a molecules. The bases of adjacent microvilli are connected by myosin-2 and spectrin in a region called the "terminal web". Bars, i - 60μm, ii - 0.6 μm.

BBs are found at the apical surface of the epithelia lining the lumens of many organs, such as the intestine, liver, kidney, and choroid plexus. BBs are highly ordered structures composed of tightly packed arrays of microvilli, cellular membrane protrusions supported by highly cross-linked, parallel bundles of actin filaments (Mooseker and Tilney, 1975). In the BB, up to ~1000 microvilli protrude from an apical surface that may only be ~100 μm^2. To accommodate the large number of protrusions, microvilli are tightly packed in an exquisite, well-ordered hexagonal pattern (Tyska et al., 2005). Microvilli are generally short (~1-5 μm long) and are supported by a bundle of ~10-30 parallel actin filaments (Tilney and Mooseker, 1971). For intestinal microvilli, the principal actin bundling proteins are fimbrin and villin (Bretscher and Weber, 1979; Bretscher and Weber, 1980a). Similar to other actin-based cellular protrusions, such as stereocilia and filopodia, the actin-rich environment within the microvillus is home to a variety of myosins (Heintzelman et al., 1994) that play key roles in maintaining the BB structure (Tyska et al., 2005). Among the most abundant are myosin-2 in the terminal web (Fig. 1-1), and myosin-1a, a class I membrane-binding motor that forms a spiraling array of lateral bridges that link the apical membrane to the underlying actin bundle (Fig. 1-1) (Tyska et al., 2005).

Myosin-1a is a divalent membrane-actin cross-linker

Although myosin-1a motor activity in the microvillus has not been examined directly, a number of this motor's properties have been extensively characterized. Myosin-1a was the first of eight vertebrate myosins-1 to be identified (Mooseker

and Coleman, 1989), and was first visualized as 'lateral arms' that link the core actin bundle to the plasma membrane in electron micrographs of the enterocyte BB (Mooseker and Tilney, 1975). This association with cellular membranes is a hallmark feature of all class I myosins (Pollard et al., 1991), and is linked to the diverse cellular functions performed by these motors (O'Connell et al., 2007). Membrane interactions are mediated by a C-terminal 'tail', which possesses a highly basic Tail Homology (TH1) domain thought to electrostatically interact with acidic phospholipids (Hayden et al., 1990); in addition, a conserved pleckstrin homology (PH) motif may specifically bind phosphoinositides such as phosphatidylinositol bisphosphate (PIP_2) (Hokanson et al., 2006). Actin binding is mediated by an N-terminal 'motor' domain that hydrolyzes ATP to produce force and movement. The N- and C-terminal domains are connected by a single alpha-helix (Fig. 1-2); this 'neck' region is supported by calmodulin light chains, and acts as a mechanical 'lever arm' (Warshaw et al., 2000) to couple conformational changes in the motor domain to a physical displacement of the membrane-binding tail domain.

Myosin-1a interactions with actin filaments

The myosin-1a motor domain contains motifs that are conserved across the myosin superfamily, such as the actin-binding site and a nucleotide binding pocket (Rayment et al., 1993). These two sites are functionally linked such that the motor has a low affinity for actin when ATP is bound, while actin affinity increases if the nucleotide pocket binds ADP or is empty (Howard, 2001). Because the motor hydrolyzes ATP into ADP (and Pi), the catalytic cycle is linked

to a cycle of attachment and detachment from actin filaments. Attachment to actin is also accompanied by a conformational change referred to as the "working stroke" that generates force and movement. Slight variations in the kinetics of nucleotide and actin binding (Fig. 1-3) can produce motors with divergent capabilities (De La Cruz and Ostap, 2004). A key parameter that defines how a particular myosin functions is the fraction of its ATPase cycle that it remains strongly bound to actin, called the duty ratio. The duty ratio is important because it is a way of describing how a motor behaves; for example, a cargo being moved along an actin filament by a motor with a low duty ratio of 5% would require 20 such motors (1/duty ratio) to be continuously bound to actin. Thus, it is thought that motors with low duty ratios normally function in large ensembles (e.g. dynein in a cilium), while high duty ratio motors function in small groups or even as single molecules (e.g. myosin-5 in vesicle transport) (Leibler and Huse, 1993).

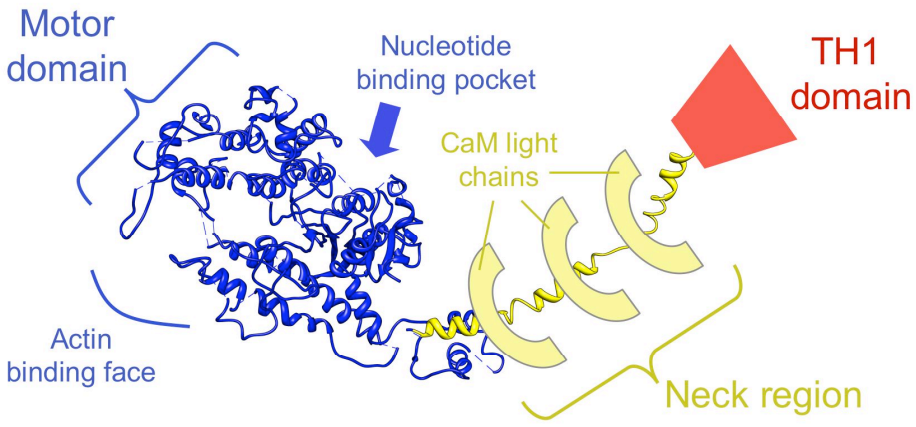

Figure 1-2. An introduction to myosin-1a structure.
Predicted structure of myosin-1a, based on homology with known protein structures (Kelley and Sternberg, 2009). All myosins-1 share a common structural arrangement: a globular N-terminal motor domain (blue) is connected to a membrane-binding tail (red) by an a-helical neck region (yellow) that is bound by CaM light chains (half moons).

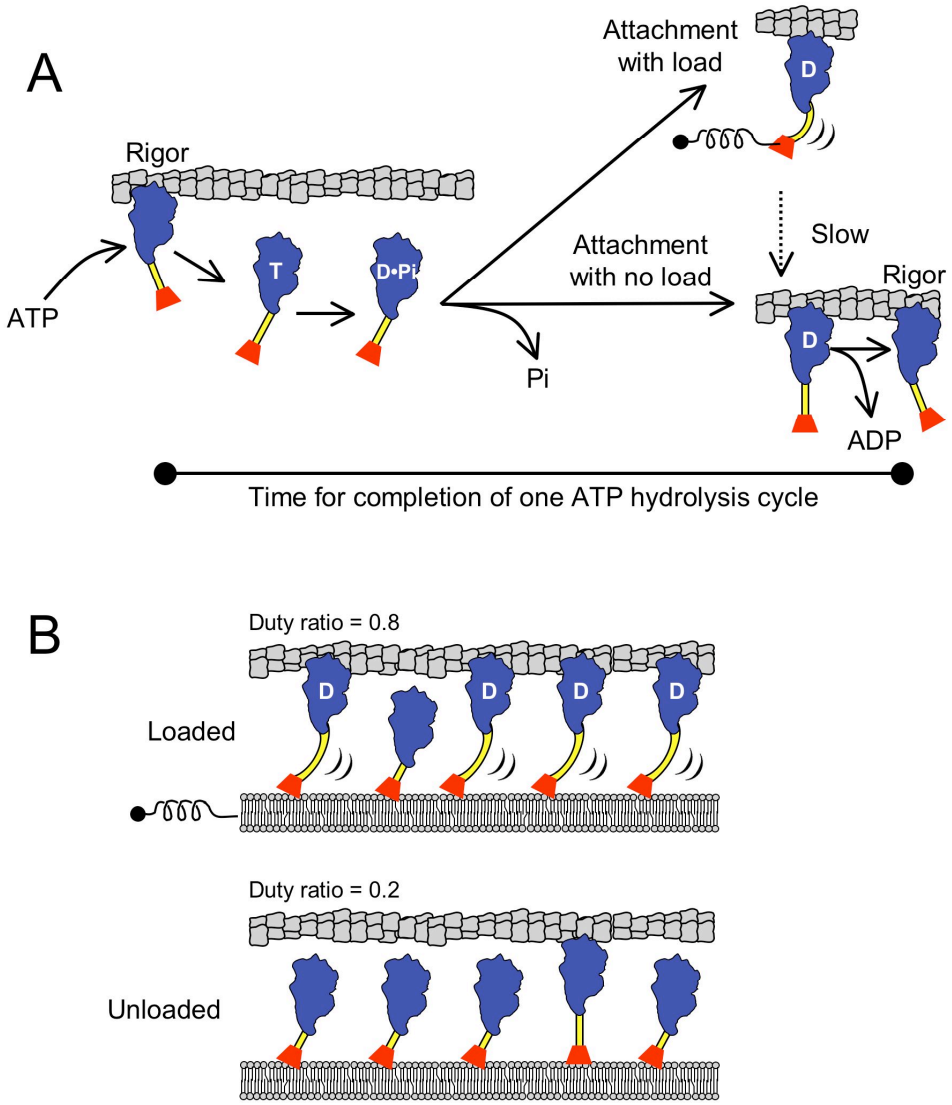

Figure 1-3. Myosin-1 mechano-chemical cycle.
(A) The myosin-1 mechano-chemical cycle. Myosin-1 bound to actin in a nucleotide-free rigor state is released when it binds ATP (T). Hydrolysis of ATP to ADP (D) and phosphate (Pi) allows myosin to bind to the actin filament, coincident with Pi release. If the motor is unloaded, ADP is rapidly released and the cycle can repeat; however, if an opposing load is present, ADP release is inhibited, and the motor stalls in a strong actin-binding state.
(B) Myosin-1 is mechanically regulated. At steady state, the fraction of myosin-1 molecules bound to actin is higher while under load, i.e. it exhibits a higher duty ratio (Laakso et al., 2008). Because myosin-1 is natively bound to cellular membranes, the ability of the tail-membrane complex to exert an opposing load will influence the actin-binding state of the motor.

Kinetic analyses of class I myosins in solution found that these motors are low duty ratio and spend the majority of their time detached from actin filaments (De La Cruz and Ostap, 2004). However, several lines of evidence suggest that these motors display more complex behavior when attached to actin filaments. Cryo-EM studies showed that myosin-1a bound to actin filaments underwent a large tail swing (~32°) upon ADP release, moving the tail domain ~6nm (Jontes and Milligan, 1997; Jontes et al., 1995). Subsequent biochemical analysis found that myosin-1a had a high ADP affinity and possessed two distinct ADP-bound states (Jontes et al., 1997); the authors suggested that the biochemical transition between these two states accompanied the structural transition observed in the cryo-EM reconstructions (Jontes et al., 1997). This hypothesis was supported by single molecule studies of myosin-1a, -1b, and –1c, which revealed a two-step working stroke: an initial ~6 nm step with a duration independent of ATP concentration (presumably ADP-bound), and a second ~5nm step with a duration sensitive to ATP concentration (presumably in rapid equilibrium between ATP- and ADP-bound) (Batters et al., 2004; Jontes and Milligan, 1997; Veigel et al., 1999).

These studies clearly demonstrate that the myosin-1a power-stroke occurs in two steps, the first occurring with actin attachment and Pi release, and the second occurring upon ADP release. Although the working stroke may simply occur in two discrete steps, studies examining smooth muscle myosin-2 suggest the more interesting possibility that a two-step stroke is actually a mechanism to sense mechanical strain (Sweeney, 1998). In this model, myosin binding to actin

initiates the first part of the working stroke. If an opposing load is present, ADP release is inhibited and the motor stalls in an actin-attached ADP-bound state until the strain is relieved. The net result is that load increases the lifetime of the myosin-actin interaction, thereby increasing the duty ratio (attached duration/total-cycle-duration). This model was recently shown to be true for myosin-1b in a recent study utilizing a fast feedback force-clamp optical trap (Laakso et al., 2008). In these experiments, a single molecule of myosin-1b displayed attachment kinetics that were exquisitely sensitive to the presence of a small opposing load (~1.5 pN), increasing its duty ratio from 0.2 in an unloaded state to 0.9 under loaded conditions (Laakso et al., 2008). While these studies were limited to myosin-1b, the presence of a two-step working stroke and biochemical similarities suggest that strain sensitivity is also present in myosin-1a and –1c (Batters et al., 2004; Jontes et al., 1997; Veigel et al., 1999). It remains to be seen how myosin-1a strain sensitivity will function *in vivo*, given that the motor is attached to a fluid lipid bilayer that may offer little or variable levels of resistance (Fig. 1-3).

Myosin-1a interactions with membranes

Myosin-1a interacts with cellular membranes via a C-terminal tail homology 1 (TH1) domain that is highly basic (pI ~9.0) due to the presence of a large number of lysines and arginines. Direct binding of a myosin-1 to cellular membrane lipids was first demonstrated biochemically with Acanthamoeba myosin-1c (Miyata et al., 1989), which showed a physiologically significant K_D of ~140 nM (Adams and Pollard, 1989). The latter study found that this motor demonstrated a strong

binding preference for acidic lipids such as phosphatidylserine and PIP_2. Similar lipid binding preferences were also observed for myosin-1a purified from chicken intestine, which showed the strongest binding to liposomes composed of negatively charged phospholipids (Hayden et al., 1990). TH1-membrane interactions can be long-lived; fluorescence recovery after photobleaching (FRAP) and transient kinetic measurements both suggest that the lifetime of a single TH1-membrane interaction may be several-fold longer than the duration of a single ATPase cycle in the absence of external loading (Tang et al., 2002; Tyska and Mooseker, 2002).

Electrostatic interactions are one well-characterized mechanism by which myosins-1 can bind cellular membranes (Adams and Pollard, 1989; Doberstein and Pollard, 1992; Hayden et al., 1990). However, an additional and more specific binding mechanism was suggested by studies showing that myosin-1c colocalized with PIP_2-enriched regions of the plasma membrane in cultured adipocytes (Huang et al., 2004) and hair cell stereocilia (Hirono et al., 2004). In an attempt to identify potential PIP_2 binding sites in myosin-1c, a recent study using a secondary structure homology algorithm found a novel pleckstrin homology (PH) motif in the TH1 domain (Hokanson et al., 2006). Despite having weak sequence similarity, the sequence present in the TH1 was structurally similar to other PH motifs, and demonstrated binding specificity for the inositol ring head group similar to that observed in canonical PH domains such as that found in PLCδ (Kavran et al., 1998). Alignments with other vertebrate myosin-1 isoforms indicate that the conserved β1-loop-β2 structure required for PIP_2

binding may be a class-wide feature. Indeed, recent work with the short-tailed motor, myosin-1g, suggests that it may target to the membrane in a PIP_2-dependent manner (Olety et al., 2009). While membrane binding is a conserved feature of all class I myosins, evidence for myosin-generated forces on cellular membranes has been decidedly lacking. In particular, it is currently unknown if the attachment to the membrane is strong enough to transmit forces from attached motors to the membrane, or if motor activity causes the tail to "slip" along the membrane surface.

Historical perspective of myosin function in the brush border

Although myosin-1a was identified as a major component of the enterocyte brush border in the 1970's (Matsudaira and Burgess, 1979; Mooseker and Tilney, 1975), myosin-1a motor activity has never been examined in the context of its native setting, the enterocyte microvillus. The reason for this is largely historical, as myosin-1a was not identified as a myosin until 1989 (Mooseker and Coleman, 1989). Between its visualization in 1975, and its identification as a motor protein in 1989, the brush border was extensively characterized biochemically and structurally (Conzelman and Mooseker, 1987; Glenney and Weber, 1980; Hirokawa and Heuser, 1981; Hirokawa et al., 1982; Howe and Mooseker, 1983; Matsudaira and Burgess, 1979). Studies of epithelial cells and tissue in culture conducted around 1970 had reported that microvilli were motile structures (Sandstrom, 1971; Thuneberg and Rostgaard, 1968), leading investigators to explore the possibility that microvilli may possess then-unknown motor proteins. In the early 1970's, studies conducted in the laboratory of Lewis Tilney showed

that the core of microvilli was composed of actin bundles (Tilney and Mooseker, 1971), and that the filaments in these bundles were uniformly polarized (Mooseker and Tilney, 1975). At around the same time, actin-based motility was shown to occur in other non-muscle systems (Perry et al., 1971; Schroeder, 1973), leading to the hypothesis that the bases of microvilli functioned in a manner similar to a muscle sarcomere, pulling the microvillar actin bundle inward (Mooseker, 1976). This movement was thought to enable microvilli to “stir” the extracellular fluid, much like the well-studied beating of cilia in the airway epithelium (Walker and Kiefer, 1966). Based on what was known about muscle physiology, myosin contraction was stimulated by adding calcium and ATP to detergent-extracted brush borders. This treatment caused two movements: a purse-string type of contraction in the terminal web region, and a shortening of the microvilli (Mooseker, 1976; Rodewald et al., 1976). The inclusion of calcium in the activation buffer turned out to be a critical experimental detail when it was shown in 1980 that the actin bundling protein villin severs actin filaments when exposed to micromolar levels of calcium (Bretscher and Weber, 1980b; Craig and Powell, 1980; Mooseker et al., 1980). Because villin was shown to fragment the microvillar actin bundle in response to the same levels of calcium present in the “activation buffer”, the descriptions of microvillar contraction were attributed to villin-induced severing of the core actin bundles (Burgess and Prum, 1982). By the time that myosin-1a was identified as a motor protein in 1989, the idea that microvilli may possess motile properties had largely been set aside, and

myosin-1a was viewed primarily as a fixed structural element that stabilized microvillus structure.

New discoveries of Myosin-1a cellular functions

Data from recent studies have challenged the view of myosin-1a as a largely static crosslinker, instead suggesting that myosin-1a plays an active role in regulating BB composition and structure. FRAP analysis of GFP-tagged constructs found that >80% of myosin-1a in the microvillus turned over rapidly (<1 min.), suggesting that the majority of these molecules are quite dynamic (Tyska and Mooseker, 2002). This study also found that a GFP-tagged myosin-1a tail construct recapitulated the localization of full-length myosin-1a; when transfected into CACO2 cells, this tail construct acted as a dominant negative, displacing the endogenous myosin-1a from the apical microvilli (Tyska and Mooseker, 2004). Strikingly, the tail construct also caused the loss of the transmembrane protein SI from microvilli, but did not disrupt the localization of the transmembrane protein aminopeptidase N (APN) or the GPI-linked protein IAP (Tyska and Mooseker, 2004). Earlier models suggesting that myosin-1a functioned in the transport of apically targeted vesicles (Fath and Burgess, 1993) are unlikely to explain these results given the specificity of this disruption. Instead, biochemical analysis revealed that the cytoplasmic N-terminus of SI directly interacts with the myosin-1a tail, suggesting that a primary function of myosin-1a is to retain specific components in the brush border (Tyska and Mooseker, 2004).

Combined with recent studies showing the strain-sensitivity of the myosin-1 power stroke (Laakso et al., 2008), the finding that a population of myosin-1a molecules interacts with a transmembrane protein suggests an interesting scenario: if the interaction between SI and myosin-1a is capable of exerting an opposing load, motors attached to SI could stall in an actin-attached state. Interactions between loaded myosin-1a and actin filaments would be predicted to be long-lived (on the order of seconds), and could explain the immobile fraction of myosin-1a molecules (~20%) observed in FRAP analysis (Tyska and Mooseker, 2002). This is an attractive possibility, given that the immobile fraction corresponds to the ~20% of myosin-1a found associated with SI-rich lipid rafts (Tyska and Mooseker, 2004). Differential attachment to the membrane could create two kinetically and mechanically distinct populations of myosin-1a molecules in microvilli: myosin-1a molecules attached via TH1 electrostatic interactions (~80%) could be low duty ratio, while those attached to SI (~20%) could exhibit a high duty ratio. One possibility is that the low duty ratio motors could apply force to facilitate movements toward the microvillus tip, while the high duty ratio motors could contribute to membrane tension by providing links between the membrane and cytoskeleton (Sheetz, 2001). Evidence for the latter function can be found in studies of the myosin-1a knockout (KO) mouse. In the KO, microvilli have non-uniform lengths and often display membrane 'herniations' where the apical membrane appears to have detached from the underlying actin cytoskeleton (Tyska et al., 2005). In agreement with the cell culture studies (Tyska and Mooseker, 2004), KO BBs also show decreased levels of SI (Tyska

et al., 2005). These abnormalities suggest that myosin-1a plays a significant role in maintaining membrane tension and in anchoring SI. While the function of the motors not bound to SI remains unclear, it is tempting to speculate that they are involved in the tipward-directed movement of microvillar components.

Summary

The goal of this dissertation is to explore the activity of myosin-1a in the enterocyte microvillus, and how this activity contributes to brush border function. Myosin-1a was the first identified vertebrate unconventional myosin, yet its cellular functions are only now beginning to be explored. Here we examine the motor activity of myosin-1a in the context of its native setting, the enterocyte microvillus (Chapter III). We find that in isolated BBs, the ensemble of myosin-1a generates substantial force directed toward the tip of the microvillus, resulting in the translation of the apical membrane toward the barbed (+) end of the actin bundle. This movement results in the release of the apical membrane from the microvillus tip in the form of small vesicles. When native tissue was examined for signs of this activity, we found that microvillar tips possessed membrane protrusions reminiscent of budding vesicles, and that these protrusions are specifically enriched in the membrane protein intestinal alkaline phosphatase (IAP). Biochemical fractionation of the contents of the intestinal lumen yielded a population of small vesicles that were also specifically enriched in IAP. Myosin-1a knock-out mice demonstrated defects in lumenal vesicle (LV) morphology and composition, suggesting that myosin-1a is a critical regulator of LV formation and/or release (Chapter IV). The enrichment of IAP in the LVs suggested that a

primary function of LVs is to deliver IAP enzymatic activity into the intestinal lumen. Because IAP has recently been shown to detoxify bacterial lipopolysaccharide (LPS) (Bates et al., 2007; Goldberg et al., 2008), we explored the possibility that LVs play a role in gut mucosal immunity. Consistent with this proposed function, we find that LVs natively interact with bacteria in the intestinal lumen, dephosphorylate purified bacterial LPS, and protect cultured epithelial cells from the toxic effects of LPS (Chapter V). Taken together these studies suggest that myosin-1a plays an active role in regulating the plasma membrane in the enterocyte brush border, including a new form of vesicle release that functions in host defense.

CHAPTER II

MATERIALS AND METHODS

Brush border isolation

BBs were collected with a modification of the method of Howe and Mooseker (1982). All procedures involving animals were carried out under the auspices of VUMC IACUC. All chemicals were from Sigma-Aldrich unless otherwise noted. Intestines were dissected from adult animals (Sprague-Dawley rats or wild type/Myo1a KO mice), flushed with ice-cold saline (150 mM NaCl, 2 mM Imidazole-Cl, 0.02% Na-Azide) and stirred in dissociation solution (DS, 200 mM sucrose, 0.02% Na-Azide, 12 mM EDTA-K, 18.9 mM KH2PO4, 78 mM Na2HPO4, pH 7.2) for 20 min. Released cells were washed with multiple cycles of sedimentation (200 x g for 10 min in a Beckman X-15R) and resuspension in fresh DS. Cleaned cell pellets were resuspended in homogenization buffer (HB, 10 mM Imidazole, 4 mM EDTA-K, 1 mM EGTA-K, 0.02% Na-Azide, 1 mM DTT, 1 mM Pefabloc-SC, pH 7.2) and homogenized in a Waring blender with 4 x 15 sec pulses. BBs were collected from the homogenate by centrifugation at 1,000 x g for 10 minutes; BB pellets were then washed in solution A (75 mM KCl, 10 mM Imidazole, 1mM EGTA, 5 mM MgCl2, 0.02% Na-Azide, pH 7.2) and sucrose added to 50% final concentration. Samples were overlayed with 40% sucrose and centrifuged at 130kg for one hour at 4°C in a Beckman L8-70M ultracentrifuge. BBs were collected from the 40%/50% interface, resuspended in

solution B (150 mM KCl, 20 mM Imidazole, 2 mM EGTA, 5 mM MgCl2, 0.02% Na-Azide, 1 mM DTT, 1 mM Pefabloc-SC, pH 7.2) and stored on ice. Protein concentrations were determined using the Coomassie Blue Assay (Pierce).

Microscopy

Confocal microscopy: Isolated BBs were incubated in solution B in the presence or absence of 2 mM ATP for 5 min at room temperature, then fixed for 15 minutes at room temperature with 4% paraformaldehyde in PBS (137 mM NaCl, 7 mM Na2HPO4, 3 mM NaH2PO4, pH 7.2). BBs were then washed with fresh PBS, stained with Alexa488-phalloidin (1:200) and either TRITC-ConA (1:200, Molecular Probes, Eugene OR) or AM1-43 (1:100, Biotium Inc., Hayward, CA) overnight on ice. BBs were washed three times in PBS and mounted on slides. Confocal micrographs were acquired on an Olympus FV-1000 (100x/1.3 N.A. Plan Apo objective). All images were contrast enhanced, pseudo-colored, and cropped using ImageJ software (v. 1.36b, NIH); figures were assembled using PowerPoint X (Microsoft). Pearson correlation values were calculated from BB confocal images as follows. Briefly, red and green color channels were separated and converted to 8-bit grey scale images. Each image was normalized with the Enhance Contrast function, such that 0.5% of all pixels achieved saturation. Correlation coefficients were then extracted using the Colocalization Finder plug-in (C. Laummonerie and J. Mutterer, IBMP, Strasbourg, France).

Time-lapse light microscopy: BBs in solution B were added to flow cells constructed of #1 cover glass (Corning) separated by two parallel strips of double-sided Scotch tape. Flow cells were imaged using a Nikon TE2000 inverted microscope equipped with either DIC optics (100x/1.3 N.A. Plan Fluor objective, CoolSnap HQ CCD camera (Roper Scientific), ImagePro Express software (Media Cybernetics)), or a QLC100 (Visitech) spinning disk confocal head (100x/1.4 N.A. Plan Apo objective, Cascade 512B CCD camera (Roper Scientific), IPLab software (BD Biosciences)). Images used to calculate velocity histogram data were acquired on a Leica TCS SP5 laser-scanning confocal (63x/1.4 N.A. Plan Apo objective). To activate BBs, solution B supplemented with 2 mM ATP was pipetted into the flow cell during image acquisition. Montages of time-lapse data were created using ImageJ v. 1.36b (NIH) and kymographs were generated using the ImageJ Multiple Kymograph plug-in (J. Rietdorf and A. Seitz, EMBL, Heidelberg, Germany).

Electron microscopy: All EM reagents were purchased from Electron Microscopy Sciences. For the ultrastructural examination of ATP-treated BBs, BBs were incubated in solution B in the presence or absence of 2 mM ATP for 5 min at room temperature. BBs were fixed in 0.1 M Na-Phosphate buffer (pH 7.0) containing 2% glutaraldehyde and 2 mg/ml Tannic acid on ice for one hour. BB were washed with 0.1 M Na-Phosphate buffer (pH 7.0) and post-fixed with 1% OsO4 in 0.1 M Na-Phosphate buffer (pH 6.0) for 30 min on ice. BBs were then washed in cold water and stained overnight in 1% uranyl acetate. Samples were then dehydrated with a graded ethanol series followed by 100% propylene

dioxide. BBs were infiltrated with a 1:1 epon:propylene dioxide mix for 6 hrs, and then placed in fresh EPON for 2 hrs and baked at 60°C overnight. Ultrathin sections were cut on a Leica ultra-microtome. For negative stain, samples were deposited on Formvar coated grids and stained with 1% uranyl acetate. All grids were imaged on a Phillips CM12 transmission electron microscope equipped with 8-bit grayscale digital image capture capabilities (1024 x 1184 pixels). For SEM, specimens were washed several times in warm HBSS, and fixed overnight at 4°C with 3% glutaraldehyde in SEM buffer (0.1 M Sucrose, 0.1 M Na-phosphate, pH 7.4). Samples were then washed in SEM buffer, post-fixed with 1% OsO_4 on ice for 1 hour, and washed in SEM buffer. Samples were then dehydrated in a graded ethanol series, dried with hexamethyldisilazane, mounted on aluminum stubs, coated with gold in a sputter coater, and viewed on a Hitachi S-4200.

Lumenal Vesicle Purification

For each LV preparation, adult Sprague-Dawley rats or adult 129 SVJ1 mice (WT and/or myo1a KO) were sacrificed and their intestines removed into ice-cold saline (150 mM NaCl, 2 mM imidazole-Cl, 0.02% Na-Azide). The intestinal contents were collected by flushing each intestine with 30-60 mL of cold saline into a beaker. The flushed material was then put through a series of centrifugation steps, with the supernatant from the preceding spin loaded into the subsequent spin: 500 *x g* for 20 min. (SX4750, Beckman); 20,000 *x g* for 30 min. (SS34, Sorvall); 100,000 *x g* for 2 hr. (70Ti, Beckman). The 100,000 *x g* pellet was then resuspended in PBS (137 mM NaCl, 7 mM Na2HPO4, 3 mM NaH2PO4, pH 7.2), layered on top of a sucrose step gradient (equal volumes of

55%, 38%, 35%, 25%, 16%, and 8% sucrose in PBS), and centrifuged at 100,000 *x g* for 16 hr. in a swinging bucket rotor (TH641, Sorvall). The gradient was then split into equal volume fractions; to remove sucrose, each fraction was diluted with 10 volumes of PBS and centrifuged at 100,000 *x g* for 2 hr. (70.1 Ti, Beckman), and the resulting pellets were resuspended in PBS.

Biochemical isolation of shed membrane

BBs (200 mg total protein) were suspended in solution B and incubated with or without 2 mM ATP for 10 minutes at room temperature. Samples were centrifuged at 5,000xg for 10 minutes at 4°C to separate shed membrane (supernatant) from intact BBs and BB fragments (pellet). To isolate the shed membrane vesicles, the 5,000xg supernatant was spun at 100,000xg for 2 hours at 4°C in a Beckman TL-100 using a TLA 120.2 rotor. 5,000xg and 100,000xg pellets were resuspended in solution B to volumes equivalent to the original reaction. The resulting fractions were prepared for immunoblot analysis and electron microscopy as described below.

BB Membrane Shedding Assay

BBs were stained with AM1-43 (1:100; Biotium Inc.) and unlabelled phalloidin (1:100, Invitrogen) overnight on ice, and then washed with fresh solution B to remove excess dye. Shedding assay reactions were carried out in triplicate; BBs were resuspended in solution B at 0.02 mg/ml and then stimulated with the addition of ATP (or other ligands as indicated) to 2 mM. Reactions were incubated for 2 min at room temperature and then subject to centrifugation at

5,000xg for 5 min at 4°C. The resulting 5,000xg supernatant was transferred to a flat-bottomed, 96-well plate (Corning) and fluorescence was measured using a Synergy HT microplate reader (Bio-Tek) using 485/15 nm excitation and 590/20 nm emission detection. Detector gain was set so that the brightest well was near the upper limit of the detector range. Control BBs (not exposed to ATP) were processed in parallel and provided an estimate of the reaction background. For each condition, the triplicate fluorescence values were averaged and background subtracted to derive the ATP-dependent response. Nucleotide analogs ATPγS and AMP-PNP were purchased from Roche Applied Science or Sigma-Aldrich.

Enzyme activity assays

To measure enzyme activity, the LV fraction was resuspended in TBS supplemented with 1 mM $MgCl_2$. Protein content was determined using a Bradford protein assay. For each reaction 100 μg of the LV fraction protein was mixed with a range of substrate concentrations in 0.2 mL TBS and incubated at 37°C for 30 minutes. All assays were measured using a Synergy HT microplate reader (Biotek, Winooski, VT). To measure alkaline phosphatase and aminopeptidase activities, the quenched fluorescent substrates 4-methylumbelliferyl phosphate and H-Leu-7-amino-4-methylcoumarin (MP Biomedical, Solon, OH) were used, respectively, and fluorescence at 460 nm measured using 360 nm excitation. Disaccharidase activities were measured by incubating 25 μg of LVs or isolated brush borders with sucrose or maltose, and the released glucose quantified using a glucose hexokinase assay (Sigma). To measure LPS dephosphorylation, 20 μL of each sample was removed and the

released phosphate measured using a malachite green assay (Baykov et al., 1988). Briefly, 0.5 mL of a 1:1 mixture of malachite green and ammonium molybdate was mixed with the sample. After one minute the reaction was quenched by adding 50 μL of 34% sodium citrate, absorbance was measured at 650 nm, and free phosphate concentration calculated from KH_2PO_4 standards.

LPS-detoxification assay

To assay LPS toxicity, purified LPS (E. *coli* O55:B5, Sigma) was incubated with or without LVs for 16hr. at 37°C. Samples were centrifuged at 100,000 *x g* (TLA 120.2 rotor, Beckman) for one hour, and the supernatant added to individual wells of 24-well plates containing confluent monolayers of cultured LLC-PK1-CL4 cells grown in 2mL αMEM (Gibco) supplemented with 10% FBS (Hyclone). After LPS addition, cells were incubated in 5% CO2 at 37°C for 5 minutes, then immediately lysed in Laemelli sample buffer. Samples were then processed for Western blot analysis as described above, using antibodies to detect total NF-κB and phospho536-NF-κB (Cell Signaling Technology, Danvers, MA). Densitometry of the Western blots was performed using ImageJ (NIH, Bethesda, MD) and the ratio of Phospho- to total NF-κB plotted in Microsoft Excel.

SDS-PAGE and immunoblot analysis

Protein fractions were separated using NuPAGE Bis-Tris 4-12% gradient gels (Invitrogen) run in Morpholineethanesulfonic acid buffer. Proteins were transferred to nitrocellulose membranes at 30V overnight at 4°C. Stock solutions of primary antibodies were used as follows: anti-Myo1a (CX-1 ascites fluid

(Carboni et al., 1988)), anti-rat SI (a generous gift from Andreas Quaroni, Cornell University), and anti-CaM (Upstate Biotechnologies) were all diluted 1:1,000; anti-AP (Sigma) was diluted 1:2,500. Secondary antibodies (Promega, Madison, WI) were diluted 1:5,000. Immunogens were visualized using ECL reagents according to manufacturer's protocol (Amersham Pharmacia Biotech).

Fluorescence Activated Vesicle Sorting (FAVS)

For FAVS analysis LVs were labeled using the following procedure: LVs were blocked for 1 hour at 4°C with 2% bovine serum albumin, labeled with anti-IAP antibody (1:400, Sigma) and DiD (1:400, Molecular Probes) for one hour at 4°C, pelleted (100,000 *x g*, 1 hour, TLA 120.2, Beckman), washed in PBS, pelleted again, resuspended in PBS, and Alexa-488 conjugated goat anti-rabbit secondary antibody was added (1:400) for 1 hour at 4°C (Molecular Probes). LVs were then pelleted, washed, resuspended in PBS, and sheared through a 27-gauge needle six times to dissociate vesicle aggregates. FAVS was performed as previously described (Cao et al., 2008). Briefly, sorting was performed using a BD Biosciences FACSAria equipped with a forward scatter PMT; linearity and sensitivity were checked using eight peak beads (Spherotech, Lake Forest, IL). Particle size resolution was determined using green fluorescent beads covering the size range of 40-700nm (Duke Scientific, Fremont, CA). A custom high-salt sheath fluid (78 mM KCl, 4 mM $MgCl_2$, 8 mM $CaCl_2$, 10 mM EGTA, and 50 mM HEPES-KOH, pH 7.0) was filtered through a 100 nm filter prior to loading into the Aria sheath reservoir. Two 200 nm in-line filters were used to assure low sheath background. Unstained and single-stained (anti-IAP

or DiD only) vesicles were used to compensate spectral overlap, which was minimal. Double stained vesicles were gated and pulse-processed to detect doublet vesicles, and individual double-positive LVs were gated to remove vesicles greater than 0.55 SD from their mean fluorescent intensities.

Mass-spectrometry analysis of FAVS-purified LVs

FAVS-purified LVs were loaded onto 10% polyacrylamide gels and samples run into the gel ~1-2 cm. The gel was then stained with Coomassie Colloidal Blue (Bio-Rad) to visualize protein, and the entire protein rich band at the top of the gel was excised, minced and treated with trypsin to generate peptides for mass analysis. LC/MS/MS analysis of the resulting peptides was performed using a ThermoFinnigan LTQ ion trap mass spectrometer equipped with a Thermo MicroAS autosampler and Thermo Surveyor HPLC pump, Nanospray source, and Xcalibur 1.4 instrument control. Samples were subjected to a reverse phase separation directly inline with the LTQ described above. The MS/MS spectra of the peptides was performed using data-dependent scanning in which one full MS spectra was followed by 3 MS/MS spectra. Peptide spectra were assigned to protein identifications using MyriMatch software (Tabb et al., 2007).

CHAPTER III

MYOSIN-1A POWERS THE SLIDING OF APICAL MEMBRANE ALONG MICROVILLAR ACTIN BUNDLES

Russell E. McConnell and Matthew J. Tyska

Department of Cell and Developmental Biology, Vanderbilt University Medical Center, Nashville, TN

Keywords: brush border, cytoskeleton, enterocyte, epithelium, vesicle

To whom correspondence should be addressed:

Matthew J. Tyska, Ph.D.
Assistant Professor
Department of Cell and Developmental Biology
Vanderbilt University Medical Center
3130 Medical Research Building III
465 21st Avenue South
Nashville, TN 37232-8240
Phone: (615) 936-5461
Fax: (615) 936-5673
Email: matthew.tyska@vanderbilt.edu

Previously published as:
McConnell, R.E., and M.J. Tyska. 2007. *Myosin-1a powers the sliding of apical membrane along microvillar actin bundles.* J. Cell Biol. 177:671-81.

Abstract

Microvilli are actin-rich membrane protrusions common to a variety of epithelial cell types. Within microvilli of the enterocyte brush border (BB), myosin-1a (Myo1a) forms an ordered ensemble of bridges that link the plasma membrane to the underlying polarized actin bundle. Despite decades of investigation, the function of this unique actomyosin array has remained unclear. Here, we show that addition of ATP to isolated BBs induces a plus end–directed translation of apical membrane along microvillar actin bundles. Upon reaching microvillar tips, membrane is "shed" into solution in the form of small vesicles. Because this movement demonstrates the polarity, velocity, and nucleotide dependence expected for a Myo1a-driven process, and BBs lacking Myo1a fail to undergo membrane translation, we conclude that Myo1a powers this novel form of motility. Thus, in addition to providing a means for amplifying apical surface area, we propose that microvilli function as actomyosin contractile arrays that power the release of BB membrane vesicles into the intestinal lumen.

Introduction

Microvilli are actin-rich membrane protrusions common to all transporting and sensory epithelial cell types. The brush border (BB) domain found at the apex of the enterocyte consists of thousands of tightly packed microvilli that extend off of the apical surface to a uniform length. In the BB, each microvillus is supported by a polarized bundle of actin filaments that are linked to the overlying apical

membrane by an ensemble of the membrane-binding motor protein, myosin-1a (Myo1a, originally brush border myosin I) (Mooseker and Coleman, 1989; Mooseker and Tilney, 1975). While the cellular role of this array remains unclear, BBs in mice lacking Myo1a demonstrate a variety of defects; among the most striking are herniations of apical membrane, irregularities in microvillar packing, and abnormal variability in microvillar length (Tyska et al., 2005). The mechanistic details underlying these phenotypes and specifically, the involvement of Myo1a motor activity, has yet to be elucidated.

Microvilli share structural features with other actin-rich membrane protrusions such as filopodia and stereocilia. In all of these cases, parallel bundles of actin filaments provide the structural core and mechanical support for the membrane extension (Revenu et al., 2004). The uniform polarity of filaments in these structures suggests that supporting bundles could serve as tracks for the polarized movement of motor proteins. Indeed, recent studies have demonstrated that myosin-X undergoes motor-driven movements toward the tips of filopodia (Berg and Cheney, 2002). In a similar manner, the motor activity of myosin-XVa is thought to drive its accumulation at the tips of stereocilia (Belyantseva et al., 2003; Rzadzinska et al., 2004). Moreover, recent data from (Yang et al., 2005) demonstrate that, in the context of the kidney proximal tubule, acute hypertension induces a redistribution in myosin-VI (Myo6) immunoreactivity from microvillar tip to base, implying that this motor may use the core bundle as a track for minus end–directed movement.

While Myo1a demonstrates mechanical activity in the sliding filament

assay (Wolenski et al., 1993b), there is currently no data on the ability of Myo1a to move apical membrane or translate membrane components along microvillar actin bundles. Based on the geometry of the microvillus (Mooseker and Tilney, 1975) and the known mechanical properties of Myo1a (Wolenski et al., 1993b), we predict that the ensemble of Myo1a in the microvillus represents a contractile array, exerting plus end–directed force on the apical membrane. In vivo, these forces could be engaged for the intramicrovillar trafficking of membrane lipids and proteins, or perhaps other unexplored roles.

We sought to test our prediction by investigating isolated BBs under conditions expected to stimulate the mechanical activity of Myo1a. Data from time-lapse imaging studies, ultrastructural analysis, and biochemical assays all indicate that the microvillar array of Myo1a is mechanically active and exerts substantial plus end–directed force on the apical membrane. In isolated BBs, this force is manifest as a rapid plus end–directed sliding of apical membrane along microvillar actin bundles. The translation of apical membrane ultimately results in the release of vesicles from microvillar tips. These studies demonstrate that microvillar actin bundles are a suitable substrate for myosin-based movement and that Myo1a produces mechanical force sufficient to power the movement of apical membrane over the actin cytoskeleton. Intriguingly, these data may also provide a mechanism for the appearance of BB membrane vesicles in the lumen of the small intestine (Jacobs, 1983). Thus, in addition to providing a means for amplifying apical surface area, we propose that microvilli function as actomyosin contractile arrays, powering the release of BB membrane vesicles into the

intestinal lumen. This activity may have implications with regard to the general efficiency of nutrient processing and other critical aspects of gastrointestinal physiology.

Results

ATP induces the redistribution of apical membrane in isolated BBs

To determine if microvillar Myo1a is mechanically active, we first examined the impact of ATP on the structure of BBs isolated from rat small intestine. For these studies, phalloidin-stabilized BBs were exposed to saturating (2 mM) levels of ATP in the presence of 1 mM EGTA; this chelator was included because Ca^{2+} is known to depress the mechanical activity of Myo1a in vitro, via effects on bound calmodulin light chains (Wolenski et al., 1993b). BBs were fixed 5 min after ATP addition, labeled with ConA, and examined using laser scanning confocal microscopy. These observations revealed that ATP treatment induced a striking accumulation of apical membrane at microvillar tips (i.e., actin bundle plus-ends; Fig. 3-1, A and B). This was confirmed quantitatively as a significant loss in the correlation coefficient calculated from the BB membrane and actin probe fluorescence signals (Fig. 3-1 C). In many BBs, we also observed terminal web contraction, an established form of myosin-II (Myo2) mechanical activity (Burgess, 1982; Keller and Mooseker, 1982; Rodewald et al., 1976).

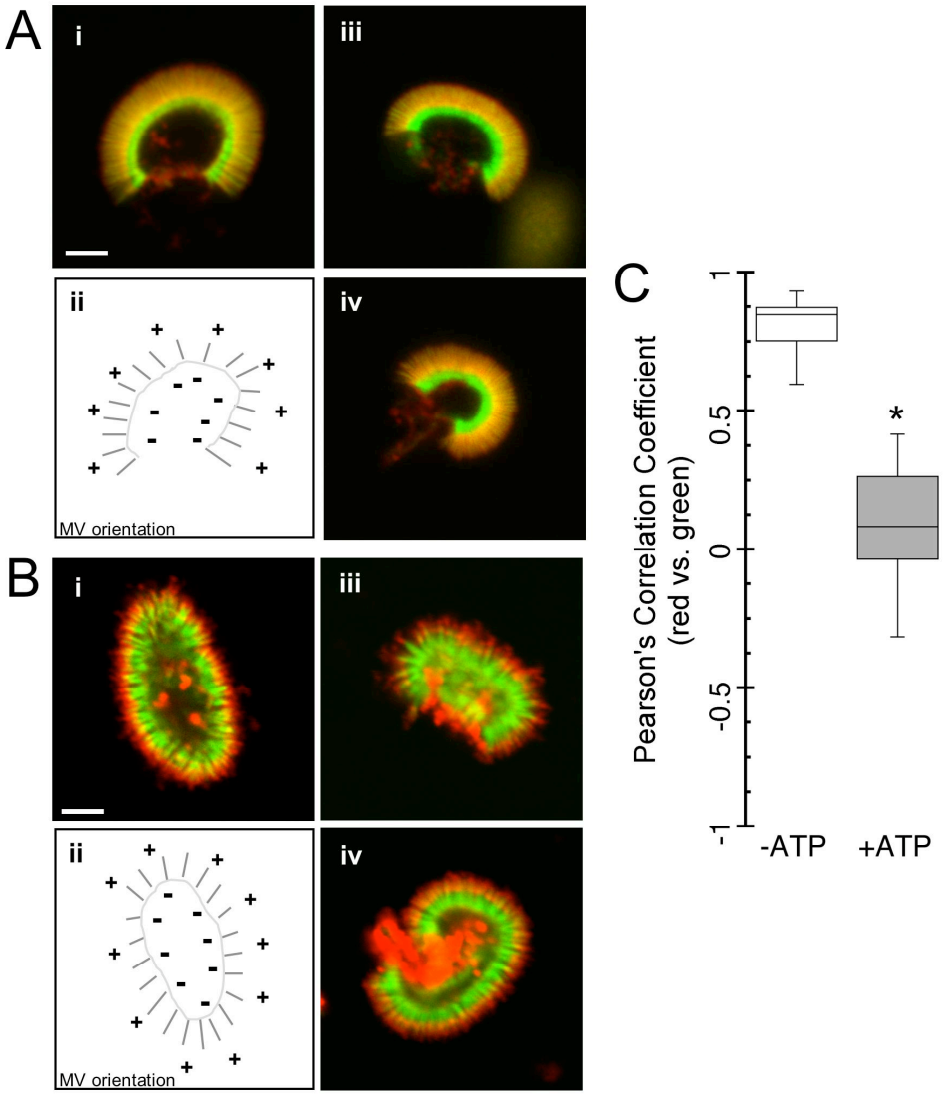

Figure 3-1. ATP induces apical membrane redistribution in isolated BBs.
(A) Laser scanning confocal sections of isolated BBs (i, iii, and iv) demonstrate the normal overlap of membrane (TRITC-ConA, red) and actin (Alexa488-phalloidin, green). **(B)** BBs treated with 2 mM ATP and then fixed 5 min later show an accumulation of membrane at microvillar tips (i.e., core bundle plus-ends). In both A and B, cartoons in panel ii show the arrangement of microvillar (MV) actin bundles for the BB in panel i. **(C)** Pearson correlation coefficients were calculated for the red (membrane) and green (actin) fluorescence images from untreated and ATP-treated BBs. Correlation coefficients are plotted as box plots; solid line within the box corresponds to the median, edges of the box are the 25th and 75th percentiles, and whiskers are the 10th and 90th percentiles. Mean coefficients were 0.81 ± 0.10 (mean ± SD, n = 14) for untreated BBs and 0.08 ± 0.21 (n = 13) for ATP-treated BBs. ATP treatment significantly reduced (*, $P < 0.00001$) the correlation between these two signals. Bars (A and B), 2.5 µm.

ATP-induced membrane redistribution is the result of plus end–directed translation

To examine the dynamics of apical membrane redistribution induced by ATP, we used time-lapse differential interference contrast (DIC) microscopy. BBs were immobilized within a flowcell and imaged with the long axis of microvilli parallel to the focal plane (Fig. 3-2, A and B). When 2 mM ATP was perfused through the flowcell we observed a robust, centrifugal expansion of the refractile bands that represent apical membrane (Fig. 3-2 C). Kymographs formed from a line that bisects the BB (Fig. 3-2 D) clearly show that the bands of apical membrane translate away from the center of the structure. Movement began immediately after ATP addition and continued rapidly in the first minute of observation. After 1 min, movement slowed as membrane reached a distance equivalent to the original position of microvillar tips (Fig. 3-2 D, white dashed lines). Although these observations suggest that ATP stimulates the translation of apical membrane along microvillar actin bundles, we sought to confirm this by performing time-lapse fluorescence microscopy of BBs labeled with probes specific to the apical membrane and actin cytoskeleton. Indeed, spinning disk confocal microscopy (SDCM) of double-labeled BBs confirmed that ATP stimulates a robust translation of apical membrane toward microvillar tips (Fig. 3-3 A and B). Kymographs of the resulting time series demonstrated that the length of microvillar actin bundles is unaffected during this process (Fig. 3-3 B).

Moreover, when the velocity of membrane movement was tallied from multiple kymographs, we obtained a mean membrane translation velocity of 19.2

± 6.1 nm/s (Fig. 3-3 C). These data indicate that ATP induces movement of apical membrane with a polarity and velocity that are consistent with the activity of a class I myosin (Coluccio, 1997).

ATP-induced membrane translation gives rise to vesiculation at microvillar tips

Kymograph analysis of SDCM time-lapse data shows that the band representing apical membrane narrows as it translates toward microvillar tips, indicating an overall loss of BB-associated membrane after ATP addition (Fig. 3-3 B). One explanation for this loss is that membrane is pushed off of microvillar tips, resulting in its vesiculation or "shedding" from the BB. Indeed, the DIC images presented above (Fig. 3-2) reveal that ATP-stimulated membrane movement is accompanied by an extensive release of material resembling small vesicles (Fig. 3-2 C, arrowheads at 68 s). Consistent with these data, SDCM images that are contrast adjusted to enable visualization of dim material reveal a cloud of vesicles in solution around the BB after ATP addition (Fig. 3-3 D). When total solution fluorescence is monitored throughout the time lapse, a burst in signal intensity is observed coinciding with the addition of ATP (Fig. 3-3 E). These data indicate that membrane shedding occurs in parallel with membrane translation.

We expect membrane shedding to take place at microvillar tips, as membrane accumulates in this region after ATP addition (Figs. 3-1, 3-2, 3-3). To further characterize the BB response to ATP and unambiguously determine the location of membrane release, we performed ultrastructural analysis on ATP-treated BBs. Transmission electron microscopy (TEM) revealed extensive vesiculation of the apical membrane at microvillar tips in the presence of ATP

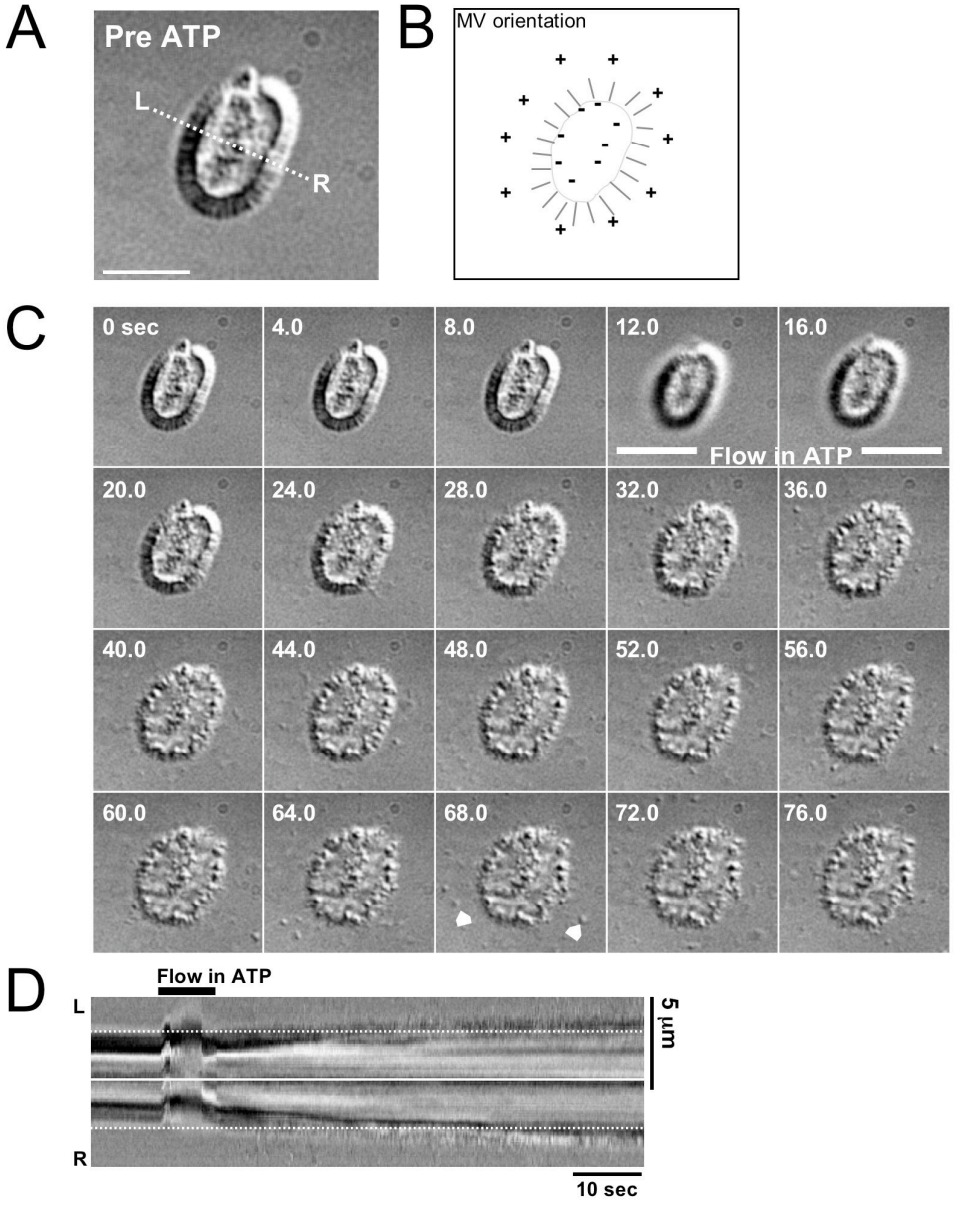

Figure 3-2. Time-lapse analysis of ATP-induced BB membrane redistribution.
(A) DIC micrograph of an isolated BB mounted in a flow cell before ATP treatment. Bar, 5 μm. **(B)** Schematic of the BB in A showing the orientation of microvillar (MV) actin bundles. **(C)** Time-lapse DIC image series of the same BB in panel A before (t = 0–8 s), during (t = 12–16 s), and after (t = 20–76 s) the addition of 2 mM ATP. Addition of ATP stimulates the translation of membrane toward microvillar tips located at the BB periphery. Membrane vesicles are also seen accumulating in solution surrounding the BB (white arrowheads at 68s). **(D)** Kymograph generated from a line drawn parallel to the microvillar axis (A, dashed line) shows movement of the BB membrane (y-axis) over time (x-axis); membrane translates away from the BB center (solid line) toward the actin plus-ends at the MV tips (dotted lines).

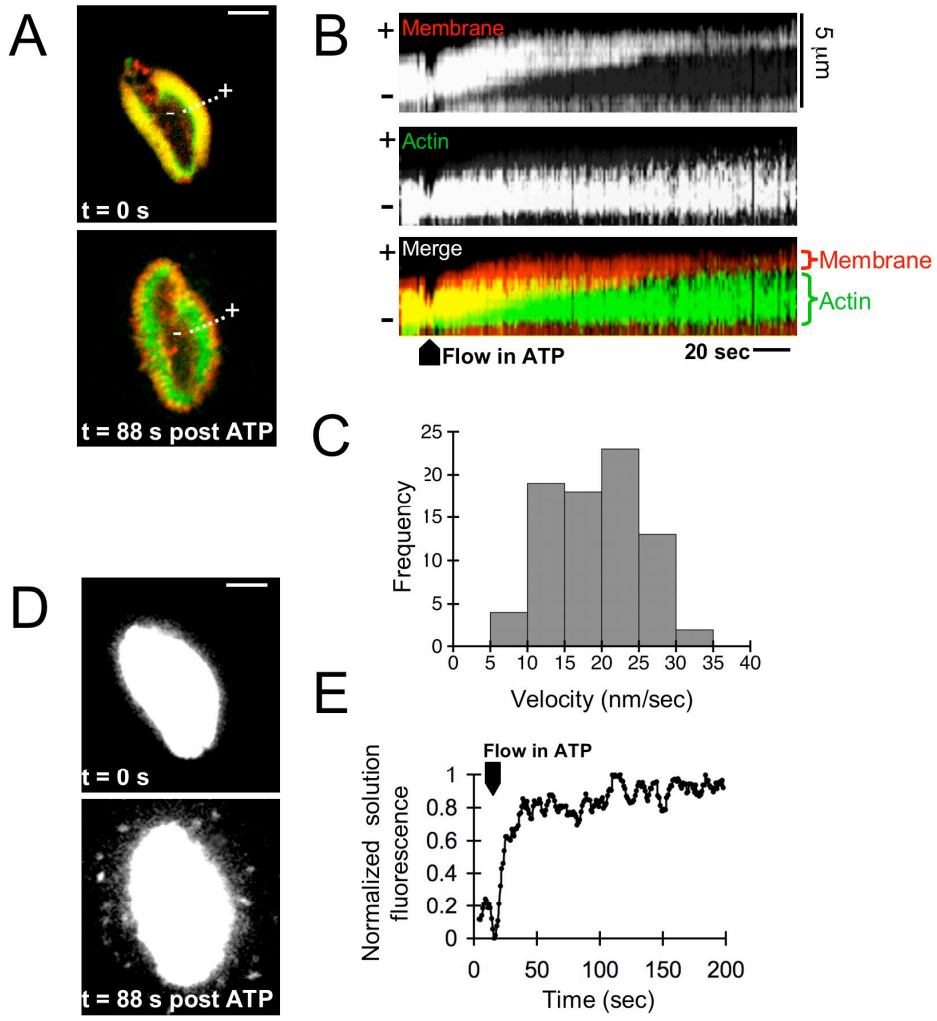

Figure 3-3. ATP stimulates the plus end–directed translation of membrane over microvillar actin bundles.
(A) Spinning disk confocal micrographs of a fluorescently labeled BB (Alexa488-ConA, membrane, red; Alexa546-Phalloidin, actin, green) before (t = 0 s) and after (t = 88s) addition of 2 mM ATP; the accumulation of membrane at microvillar tips can clearly be observed after ATP addition. **(B)** Kymographs drawn from the white dashed line over the BB in panel A reveal that membrane (red) moves toward the microvillar tips as the actin bundle length (green) remains constant. **(C)** Histogram of membrane translation velocities derived from 79 kymographs of 42 BBs; mean velocity equals 19.2 ± 6.1 nm/s (mean ± SD). **(D)** Contrast enhancement of the membrane (red) channel in panel A reveals an accumulation of small membrane vesicles in solution around the BB after ATP treatment. (E) Quantification of integrated fluorescence in solution surrounding the BB shows a release of membrane that begins immediately after the addition of 2 mM ATP. Bars (A and D), 5 μm.

(Fig. 3-4, A and B). Vesiculation was widespread and observed at the tip of nearly every microvillus (Fig. 3-4 C). High magnification panels revealed that vesiculating membrane was devoid of electron-dense material and exhibited a diameter comparable to that of the microvillus (100 nm; Fig. 3-4 D). ATP treatment also resulted in the exposure of a greater length of actin bundle at the base of microvilli. In the absence of ATP, microvillar actin bundles typically extend into the terminal web by only a small fraction of their total length (10–20% of total length; Fig. 3-4 A, red region). After ATP activation, microvillar bundles in most BBs were observed with 50% of their total length exposed and extending into the terminal web (Fig. 3-4 B, red region). In other cases, we observed actin bundles that were completely stripped of membrane, yet positioned adjacent to an accumulation of vesicles (unpublished data). These ultrastructural analyses show that ATP-induced membrane translation gives rise to membrane shedding from microvillar tips

Characterization of vesicles released during ATP-induced membrane shedding

Our ultrastructural observations suggest that the vesicles released from microvillar tips after ATP treatment represent parcels of apical membrane. To further characterize the composition and properties of shed vesicles, we used differential centrifugation to fractionate ATP-treated BBs. When BBs were incubated in the presence or absence of ATP and then sedimented at 5,000 *g*, membrane markers (sucrase-isomaltase [SI] and alkaline phosphatase [AP]) and Myo1a were released into the supernatant only in the presence of ATP (Fig. 3-5 A). Moreover, all of the SI and AP in the 5,000-*g* supernatant sedimented at

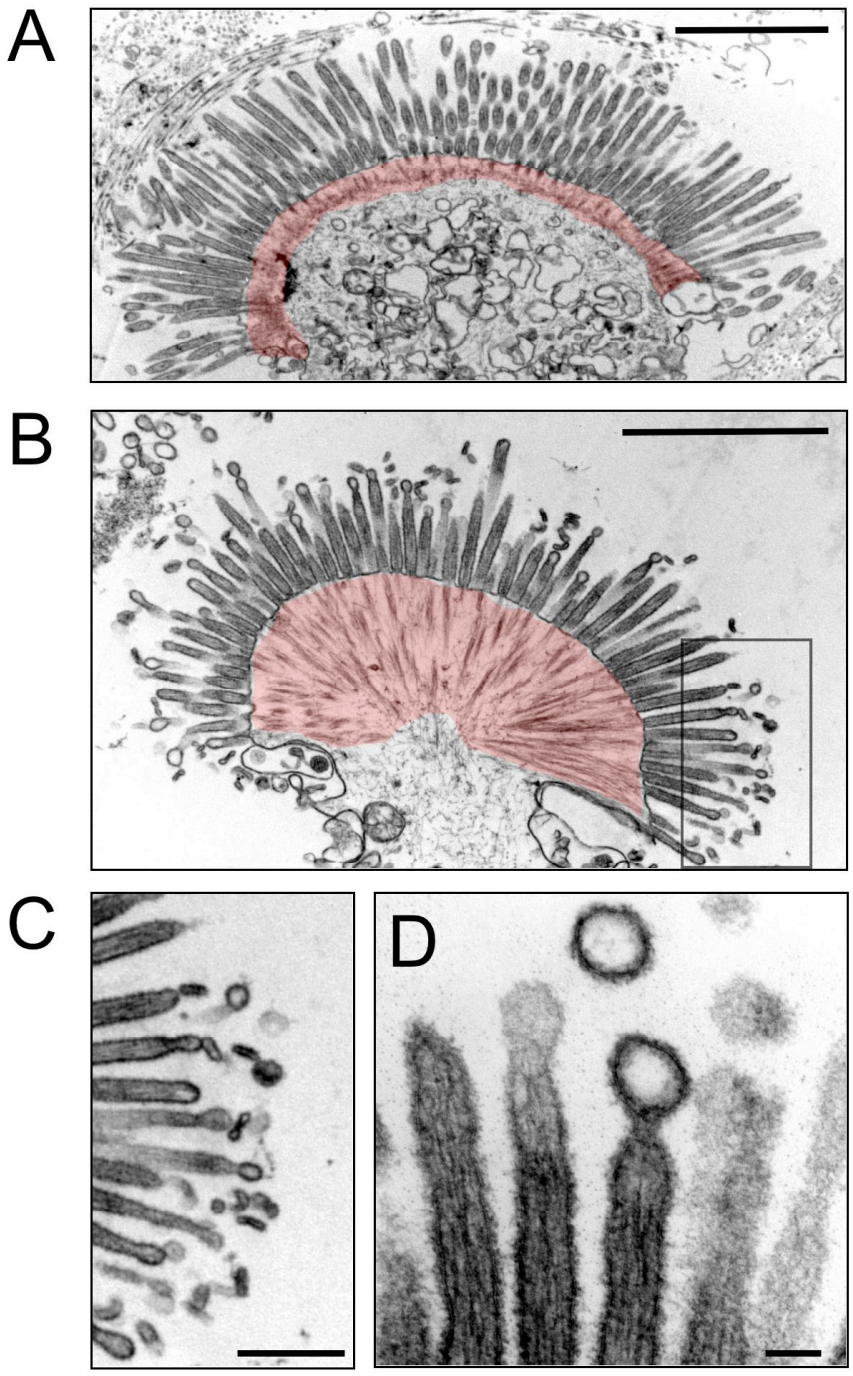

Figure 3-4. Ultrastructural analysis of BB membrane shedding.
(A) TEM analysis of an isolated BB shows that the apical membrane covers the majority of the core actin bundles, leaving only a small fraction of their length exposed at bundle minus-ends (region highlighted in red). **(B)** BB from the same preparation as in panel A after treatment with 2 mM ATP. In addition to extensive vesiculation at microvillar tips, a significantly greater length of individual actin bundles appear to be exposed (i.e., membrane free) at the bundle minus-ends (compare red regions in A and B). **(C)** Higher magnification view of boxed area in panel B clearly shows vesiculation at the tips of nearly all microvilli. **(D)** Vesicles shed from tips exhibit a diameter comparable to the microvillus and show no evidence of actin bundle fragments at their core. Bars: (A and B) 2 μm; (C) 0.5 μm; (D) 0.1 μm.

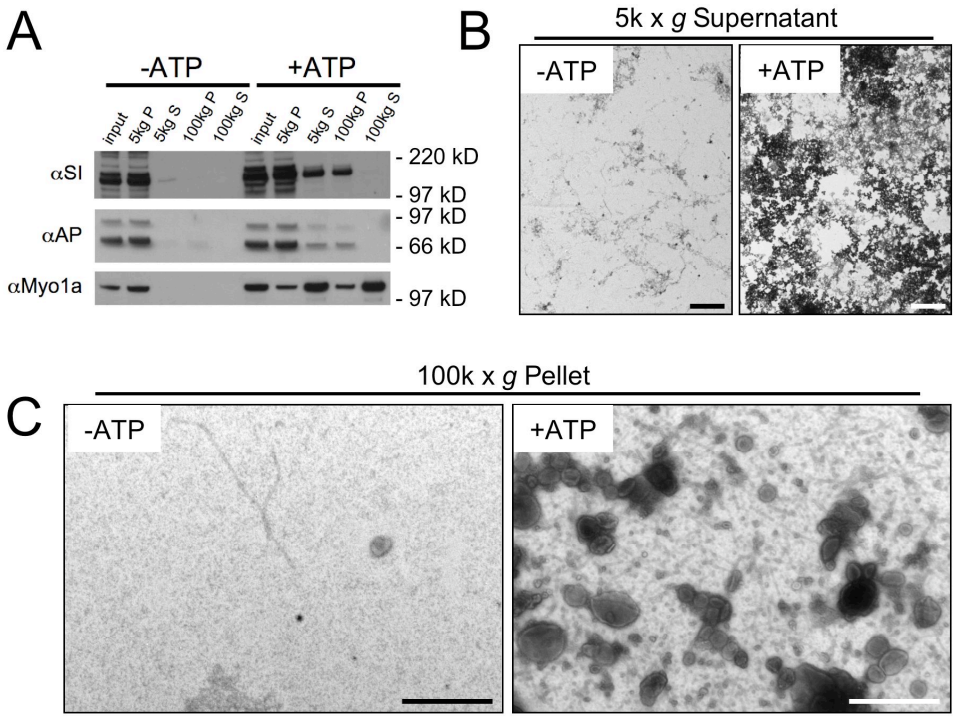

Figure 3-5. Characterization of vesicles released from the BB upon ATP treatment.
(A) BB samples in the presence or absence of ATP were fractionated using differential centrifugation and then separated using SDS-PAGE. Western blots show that apical membrane markers, SI and AP, undergo ATP-induced redistribution from the low speed (5,000 *g*) pellet (P) into the low speed supernatant (S). Ultraspeed centrifugation (100,000 *g*) of the 5,000-*g* S fraction reveals that both membrane markers sediment, indicating membrane association. Although Myo1a is also released from the BB in the presence of ATP, a significant amount of Myo1a sediments with membrane markers in the 100,000-*g* P fraction. **(B)** TEM of the negatively stained 5,000-*g* S fraction shows that ATP induces the release of copious amounts of membrane material. **(C)** TEM of negatively stained 100,000-*g* P fraction confirms the presence of small vesicles similar in appearance to those observed in micrographs of isolated BBs. Bars: (B) 2 μm; (C) 0.5 μm.

100,000 *g*, suggesting that these components are indeed membrane associated (Fig. 3-5 A). A significant fraction (20%) of the Myo1a released with ATP addition also sedimented at 100,000 *g*, indicating that a subpopulation of this motor remains bound to the apical membrane during the time course of ATP-induced membrane translation and shedding (Fig. 3-5 A). The appearance of vesicles in ATP-treated preparations was also confirmed using TEM analysis; an abundance of vesiculated membrane material appeared in the 5,000-*g* supernatant only after BBs were treated with ATP (Fig. 3-5 B). In addition, examination of the 100,000-*g* pellet showed that this fraction is enriched in small vesicles ranging from 50–200 nm in diameter, comparable to those observed in ultrastructural analyses of ATP-treated BBs (Fig. 3-5 C).

A quantitative assay for BB membrane shedding

To further investigate the mechanism of BB membrane shedding, we devised a quantitative membrane shedding assay (MSA). This assay allowed us to quantify the release of apical membrane vesicles produced by a large population of BBs, under a variety of biochemical conditions and perturbations. BBs were labeled with the lipophilic fluorescent dye AM1-43 and then activated to shed with the addition of ATP. After 2 min, vesiculated membrane was separated from BB remnants with a centrifugation step and the resulting supernatant transferred to a 96-well microplate for the measurement of AM1-43 fluorescence (Fig. 3-6 A). Importantly, AM1-43 labeling appeared uniform within and between individual BBs (Fig. 3-6 B), and the ATP-dependent signal scaled linearly with the quantity of BB in the reaction (Fig. 3-6 C).

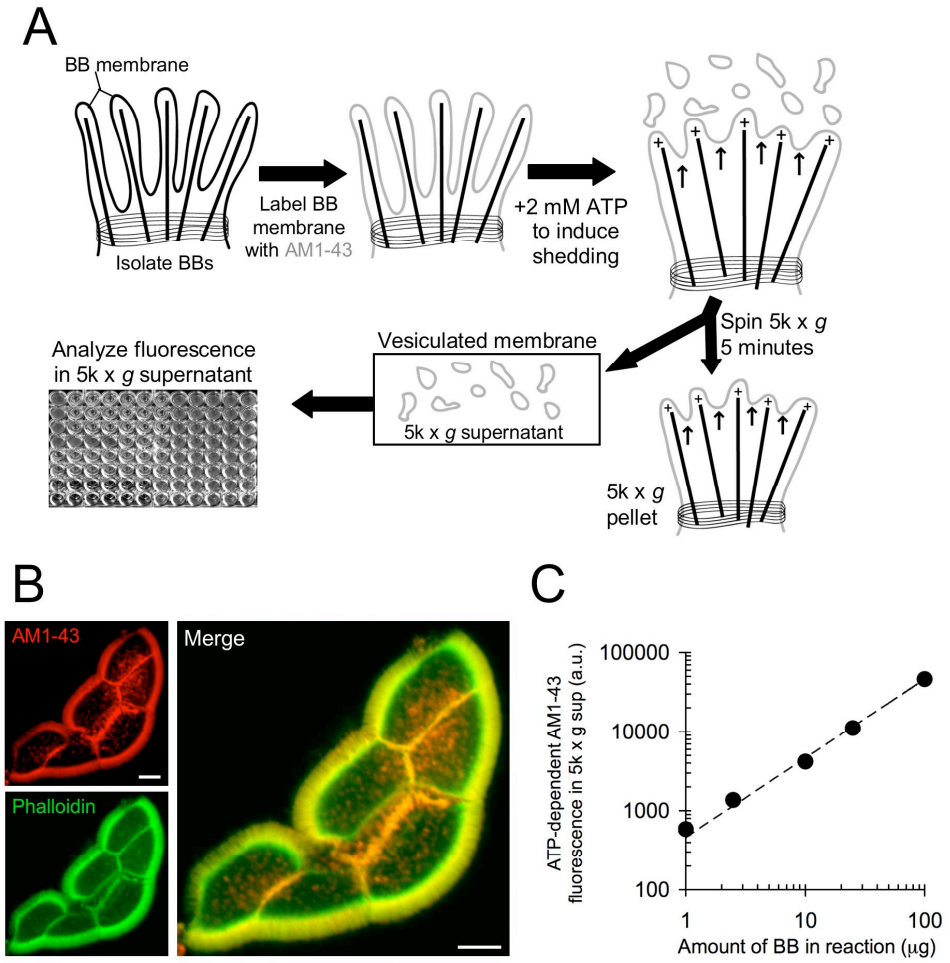

Figure 3-6. Quantitative assay for BB membrane shedding.
(A) Schematic of the assay used to quantify the extent of BB membrane shedding under various conditions. BBs are labeled with AM1-43, reacted with 2 mM ATP, centrifuged to isolate the shed membrane (5,000-*g* supernatant), and the amount fluorescent material is measured in a microplate reader. **(B)** Laser scanning confocal micrograph of phalloidin-labeled (green) isolated BBs shows that AM1-43 (red) evenly labels the BB membrane. Bars, 4 μm. **(C)** Increasing concentrations of BBs were treated with 2 mM ATP and the amount of membrane shed from each sample was measured using the microplate assay. ATP-induced membrane shedding scales with the BB concentration, demonstrating a linear response over two orders of magnitude. Points on this plot represent mean ± SD calculated from replicates at each BB concentration (for all values, SD is smaller than the point size).

BB membrane shedding exhibits the nucleotide dependence expected for a myosin-driven process

To determine if ATP-induced membrane translation and shedding are powered by an ATPase such as Myo1a, we used the MSA to examine the nucleotide dependence of this activity. In the absence of ATP, ADP and PPi were unable to activate membrane shedding (Fig. 3-7 A). Next, we determined if ATP hydrolysis was required to activate membrane shedding by carrying out the MSA with the nonhydrolyzable ATP analogues, ATPγS and AMP-PNP. These analogues produced only a fraction of the response observed for an equivalent concentration of ATP, indicating that hydrolysis is required to fully activate membrane shedding (Fig. 3-7 A). The remnant response observed in the case of both analogues (10–20% of ATP control) could be due to the low concentration of contaminating ATP in these analogue preparations. Alternatively, it may indicate that ATP binding alone accounts for a small fraction of total membrane shedding.

Myosin mechanical activity is known to demonstrate Michaelis-Menten dependence with respect to ATP concentration (Howard, 2001). If BB membrane shedding is powered by a motor such as Myo1a, it should also demonstrate such dependence. To test this, we examined the rate of membrane shedding over a wide range of ATP concentrations. Indeed, these experiments revealed that shedding (Fig. 3-7 B) exhibits hyperbolic dependence with respect to ATP concentration. Fitting these data to a Michaelis-Menten model (normalized shedding = $V_{Max}^{*}[ATP]/K_M + [ATP]$) yields a V_{Max} of 1.2 ± 0.1 mM and a K_M (for ATP) of 396 ± 103 μM. We also examined the impact of the hydrolysis product,

ADP, on shedding activity in the presence of saturating levels of ATP. In vitro biochemical studies on other myosin motors have established that ADP serves as a pure competitive inhibitor of ATPase activity (Kelemen, 1979). Consistent with this prediction, the presence of 2 mM ADP increased the K_M with respect to ATP approximately fivefold, while V_{Max} was unaffected (Fig. 3-7 B, inset). This shift in K_M enabled us to calculate an ADP K_I of 554 μM (from $K_I = K_M [ADP]/K_M' – K_M$). This value is slightly higher but comparable to that determined for smooth muscle Myo2 (in the sliding filament assay), a myosin that exhibits high affinity for ADP in a manner similar to Myo1a (Cremo and Geeves, 1998; Jontes et al., 1997; Warshaw et al., 1991).

ATP-induced membrane shedding is independent of Myo2 activity

The nucleotide dependence of membrane shedding suggests that this process is powered by a myosin ATPase. Thus, we wanted to determine if Myo2, the most abundant myosin in the BB, plays a role in driving this activity. For these experiments, we performed the MSA in the presence of 50 μM blebbistatin, an established Myo2 inhibitor (Kovacs et al., 2004; Straight et al., 2003). Consistent with the known localization of Myo2 in the terminal web, blebbistatin had no observable impact on the extent of membrane shedding from microvillar tips (Fig. 3-7 C). Moreover, in the presence of blebbistatin, BBs lacked the tight curvature normally produced by ATP addition (compare Fig. 3-7 D with Fig. 3-4 B), indicating that terminal web contraction (Burgess, 1982; Keller et al., 1985; Keller and Mooseker, 1982; Rodewald et al., 1976), and thus Myo2 activity, were

indeed inhibited. These data indicate that ATP-induced membrane translation and shedding are Myo2-independent activities.

ATP-induced membrane shedding is Myo1a dependent

Given its established membrane binding potential (Hayden et al., 1990; Zot, 1995), high density in the microvillus (Bretscher, 1991), and polarity of movement (Wolenski et al., 1993a), Myo1a is the most obvious candidate for powering the plus end–directed movement and shedding of membrane induced by ATP. Indeed, our previous studies have shown that BBs from Myo1a knock-out (KO) mice are not "damaged" to the same extent as wild-type (WT) BBs when exposed to ATP (Tyska et al., 2005). Thus, we investigated the involvement of Myo1a in the membrane shedding response by performing the MSA with BBs isolated from the small intestine of Myo1a knock-out (KO) mice (Tyska et al., 2005) and age-matched wild-type (WT) controls (Fig. 3-7 E). Strikingly, the shedding response of Myo1a KO BBs was only a small fraction (5%) of that exhibited by WT BBs (Fig. 3-7 F). The difference in activity was not due to disparity in AM1-43 labeling efficiency as labeled WT and KO BBs exhibited comparable levels of fluorescence (Fig. 3-7 G). Moreover, visual observation of the response to ATP confirmed that KO BBs failed to carry out the plus end–directed membrane translation and shedding normally observed in WT BBs (Fig. 3-7 H). Together these data strongly indicate that Myo1a is required for the ATP-stimulated membrane movement and vesiculation observed in isolated BBs.

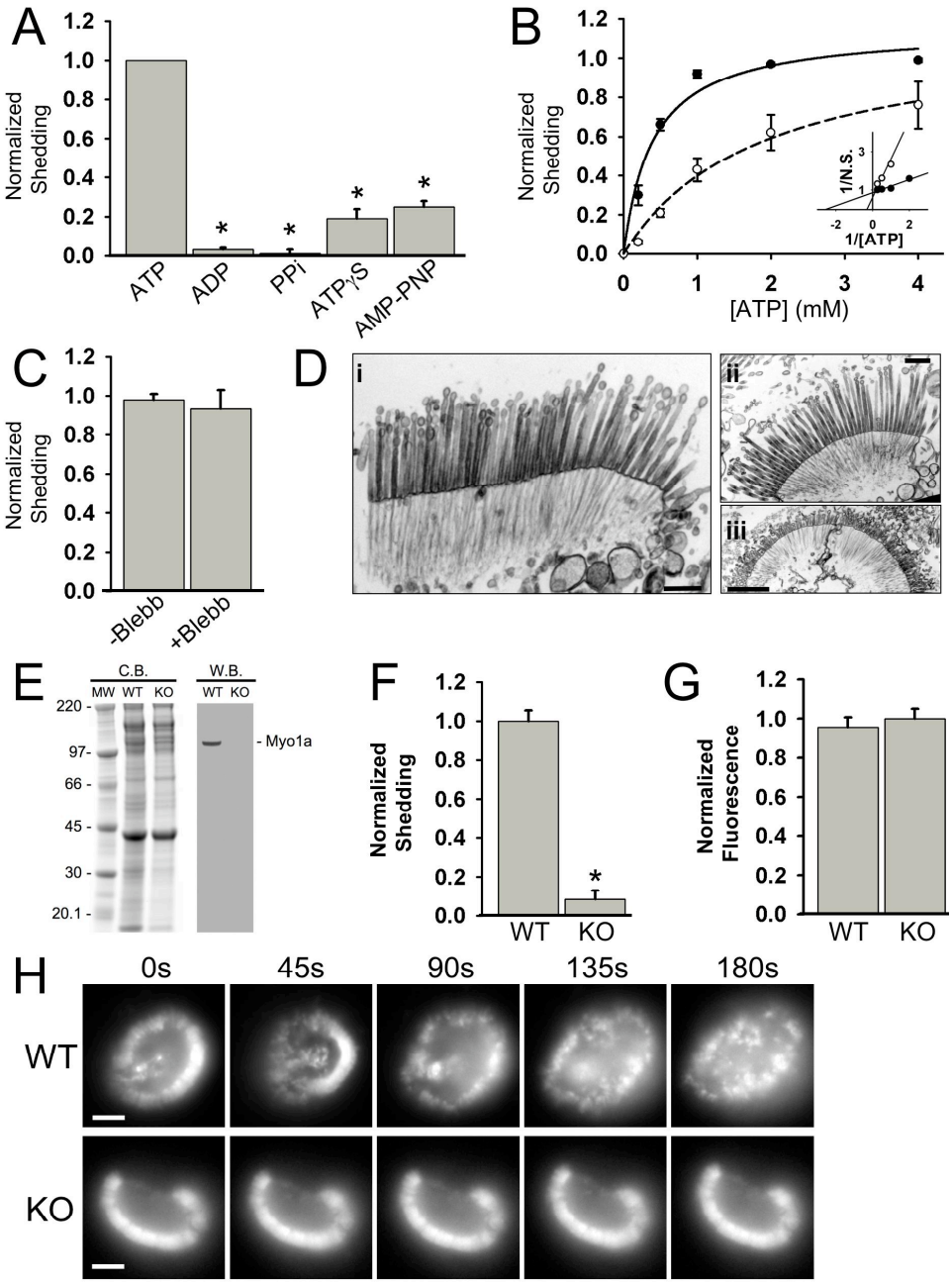
A
Normalized Shedding
1.2
1.0
0.8
0.6
0.4
0.2
0.0
ATP
ADP
PPi
ATPγS
AMP-PNP
B
Normalized Shedding
[ATP] (mM)
1/N.S.
1/[ATP]
C
Normalized Shedding
-Blebb
+Blebb
D
i
ii
iii
E
C.B.
W.B.
MW WT KO
WT KO
220 -
97-
66 -
45 -
30 -
20.1 -
- Myo1a
F
Normalized Shedding
WT KO
G
Normalized Fluorescence
WT KO
H
0s
45s
90s
135s
180s
WT
KO

Figure 3-7.

Discussion

A novel contractile activity in the microvillus

In this paper, we describe a novel form of microvillar contractility that can be reactivated by exposing native, isolated BBs to ATP. Reactivation is manifest as the plus end–directed movement of apical membrane along microvillar core actin bundles, and eventually, the accumulation of membrane at microvillar tips. Upon reaching the tips, the membrane no longer maintains contact with the underlying actin cytoskeleton and vesiculation is favored; small vesicles that contain Myo1a and are enriched in other apical membrane markers are released into solution

Figure 3-7. Nucleotide and myosin dependence of BB membrane shedding.
(A) 20 µg/ml BBs were treated with 2 mM of ATP, adenosine diphosphate (ADP), pyrophosphate (PPi), adenosine 5'-[-thio] triphosphate (ATPS), or adenosine 5'-[ß,-imido] triphosphate (AMP-PNP), and membrane shedding was quantified using the MSA. ATP strongly stimulated membrane shedding, while ADP and PPi had essentially no effect, and the nonhydrolysable ATP analogues ATPS and AMP-PNP evoked only minor responses. **(B)** Membrane shedding exhibits Michaelis-Menten kinetics with respect to ATP concentration (closed circles, solid line shows curve fit; V_{Max} = 1.2 ± 0.1 mM, K_M = 396 ± 103 µM). In the presence of 2 mM ADP (open circles, dashed line shows curve fit; V_{Max} = 1.1 ± 0.1 mM, K_M = 1,869 ± 437 µM), membrane shedding is inhibited. Inset shows the double-reciprocal plot of the same data. **(C)** Incubating BBs with 50 µM Blebbistatin, a potent Myo2 inhibitor, has no effect on membrane shedding as measured in the MSA. **(D)** TEM analysis of BBs incubated with 50 µM Blebbistatin and 2 mM ATP (i–iii) shows that the junctional contraction associated with Myo2 activity is absent, as indicated by the parallel orientation of microvillar actin bundles in these BBs (compare with Fig. 4-3). However, the robust vesiculation at microvillar tips appears unaffected by Blebbistatin. **(E)** Coomassie blue (C.B.)–stained gel of WT and Myo1a KO BB fractions and associated anti-Myo1a Western blot (W.B.) confirms the absence of Myo1a in KO samples. **(F)** ATP-induced membrane shedding measured for equal quantities (5 µg) of WT and Myo1a KO BBs. KO BBs exhibit 5% of the shedding activity seen in WT BBs. **(G)** The fluorescence signals measured from equal amounts (5 µg) of WT and Myo1a KO BBs show equivalent labeling by AM1-43. **(H)** BB membranes were fluorescently labeled with Alexa488-ConA, treated with 2 mM ATP, and imaged for 3 min. Time-lapse images show that the WT BB exhibits a robust loss of membrane, yet the KO BB membrane structure remains essentially unchanged during this time course. For the values plotted in A–C, each point represents the mean ± SD calculated from at least three different BB preparations. The values plotted in F and G represent mean ± SD calculated from replicates of the same BB preparation, but are representative of five individual paired WT and KO BB preparations. Bars: 0.5 µm (di, ii); 2 µm (diii, h). *, $P < 0.05$.

(Fig. 3-8 A). The translation and shedding of membrane requires ATP hydrolysis, demonstrates the nucleotide dependence expected for a myosin ATPase, and is substantially depressed in the absence of Myo1a. Intriguingly, the membrane translation velocities (Fig. 3-7 B; 19.2 ± 6.1 nm/s) measured here are nearly identical to velocities measured in sliding filament assays with Myo1a immobilized on lipid-coated coverslips (Wolenski et al., 1993b). Myo1a is a good candidate for driving this novel form of motility, as previous studies have established that this motor can bind directly to apical membrane lipids (Hayden et al., 1990; Zot, 1995) and proteins (Tyska and Mooseker, 2004), is present at a very high concentration (>70 μM) in the microvillus (Bretscher, 1991), and moves toward the plus-ends of actin filaments in vitro (Wolenski et al., 1993a). Thus, in combination with previous studies, our data strongly indicate that Myo1a is the motor that powers ATP-stimulated membrane translation and shedding in isolated BBs.

Our findings demonstrate that the polarized actin bundles that support microvilli serve as tracks for myosin-based motor activity. Although these studies focus on Myo1a, a reasonable extension of this is that other myosins in the BB (Heintzelman et al., 1994) may also use core actin bundles as tracks for directed transport. Consistent with this idea, recent studies in the context of kidney proximal tubule reveal that hypertension induces the redistribution of Myo6 immunoreactivity along the microvillar axis (Yang et al., 2005). Our data also show that microvillar Myo1a is mechanochemically active and generates force in its native environment. This suggests that Myo1a may function as more than a

passive "linker" serving to stabilize membrane/cytoskeleton interactions (Tyska et al., 2005). Finally, while general models for myosin-I function have always included some form of mechanical activity involving membrane rearrangement or movement (Coluccio, 1997; De La Cruz and Ostap, 2004), direct evidence for these functions has been lacking. The data presented here demonstrate directly, in a native system, that Myo1a is capable of producing mechanical forces sufficient to power the movement of cellular membranes over the actin cytoskeleton.

Physiological significance of BB membrane shedding

A number of previous biochemical studies have documented the existence of small vesicles in the lumen of the small intestine (Black et al., 1980; DeSchryver-Kecskemeti et al., 1989; Eliakim et al., 1989; Halbhuber et al., 1994; Jacobs, 1983; van Niel et al., 2001). Although these vesicles are enriched in nutrient-processing enzymes (e.g., SI and AP) in a manner similar to BB membrane, their mechanism of release remains unclear. Vesiculation from the tips of microvilli has also been captured in ultrastructural studies of intact enterocytes (Dougherty, 1976), suggesting that lumenal vesicles may originate from microvillar membrane. We propose that the Myo1a-dependent mechanical activity described in this paper provides a mechanism for the formation and release of vesicles from enterocyte BBs in vivo (Fig. 3-8 B). This model becomes even more appealing if we consider that membrane shedding from microvilli in vivo is accelerated when enterocytes are treated with antibodies against SI (Lorenzsonn and Olsen, 1982), a transmembrane disaccharidase that interacts directly with Myo1a in a raft-like

complex in the microvillar membrane (Tyska and Mooseker, 2004). The shedding of vesicles from the plasma membrane is a well-documented activity performed by a variety of epithelial cell types under normal and pathological conditions (Beaudoin and Grondin, 1991). In the gastrointestinal tract, the release of membrane vesicles laden with nutrient-processing enzymes could serve to increase the effective apical membrane surface area; such vesicles would allow processing to begin before nutrients reached the actual surface of the enterocyte (Jacobs, 1983). Others have proposed that BB membrane shedding may allow the enterocyte to continually modify its apical membrane composition (Halbhuber et al., 1994). This form of plasticity may be a critical aspect of the enterocyte response to the shifting demands in nutrient processing and absorption that are commonplace in the small intestine.

Does the membrane shedding process described here represent a general function for microvilli found on other polarized cell types? Although the expression of Myo1a is restricted to the gastrointestinal tract and inner ear (Donaudy et al., 2003; Dumont et al., 2002; Skowron et al., 1998; Skowron and Mooseker, 1999), other closely related class I myosins (Myo1b, Myo1c, and Myo1d) are more widely expressed in polarized cells from a variety of tissues (including kidney, liver, and pancreas) and in some cases are known to localize to microvilli (Coluccio, 1997). Interestingly, previous studies have established that all of these tissues release vesicles into their lumens (Beaudoin and Grondin, 1991). Thus, further studies are required to determine whether the activity described in this paper represents a general function for class I myosins

expressed in other cell types, or a phenomenon specific to the gastrointestinal tract.

In recent studies with the Myo1a KO mouse, we observed herniations of the apical domain, where large regions of BB membrane were detached from underlying microvillar actin bundles (Tyska et al., 2005). We originally proposed that these herniations arise due to a lack of membrane/cytoskeleton adhesion normally provided by Myo1a. However, our new findings suggest an alternative explanation: herniations may represent excess apical membrane in the BB. In KO enterocytes, the apical sorting machinery continues to deliver apical domain components to the BB. However, in the absence of Myo1a and its associated plus end–directed mechanical activity, membrane release from microvillar tips may be slowed, resulting in the accumulation of membrane in the BB, and ultimately the formation of membrane herniations.

The microvillar tip complex in BB membrane shedding

Early ultrastructural studies of the enterocyte BB revealed the presence of a prominent electron-dense plaque at the distal tips of microvilli (Mooseker and Tilney, 1975). To date, the role of the tip complex remains unclear, but by analogy to similar structures in stereocilia and filopodia, we suspect that at least one function may be in controlling the dimensions and dynamics of the core actin bundle (Lin et al., 2005). Does the tip complex also play a role in the process of membrane vesiculation from microvillar tips as described in this paper? It remains possible that an additional role for this complex may be in the formation of vesicles, perhaps through promoting and/or stabilizing the high curvature of

membrane that envelops the microvillus tip. This would be analogous to the activity of viral proteins such as VSV-M, which are known to be involved in curving membrane through direct interactions with lipids (Solon et al., 2005). Alternatively, this complex may contain proteins that actively promote fission and vesicle release. In either case, the tip complex must be dynamically reassembled after vesicle release or somehow left behind during the process. The former idea finds support in recent proteomic studies (van Niel et al., 2001), which show that one of the few proteins known to localize to microvillar tips, Eps8 (Croce et al., 2004), is found in vesicles released from the apical surface of cultured intestinal epithelial cells.

The BB contains two actomyosin contractile arrays

Early experiments with isolated BBs established that ATP induced a contraction of the junctional band of actin filaments surrounding the terminal web region (Rodewald et al., 1976). A number of groups actively investigated this contractility and the involvement of Myo2, which at the time was the only known force generator in the BB (Burgess, 1982; Keller et al., 1985; Keller and Mooseker, 1982; Rodewald et al., 1976). The findings presented here demonstrate that terminal web contraction and microvillar membrane translation/shedding are independent and separable activities (Fig. 3-7, C and D). Thus, we propose that the BB contains two distinct actomyosin contractile arrays: (1) a Myo2-based array that powers the contraction of the junctional band surrounding the terminal web region, and (2) a Myo1a-based array in microvilli that exerts plus end–directed forces on the apical membrane (Fig. 3-8 A).

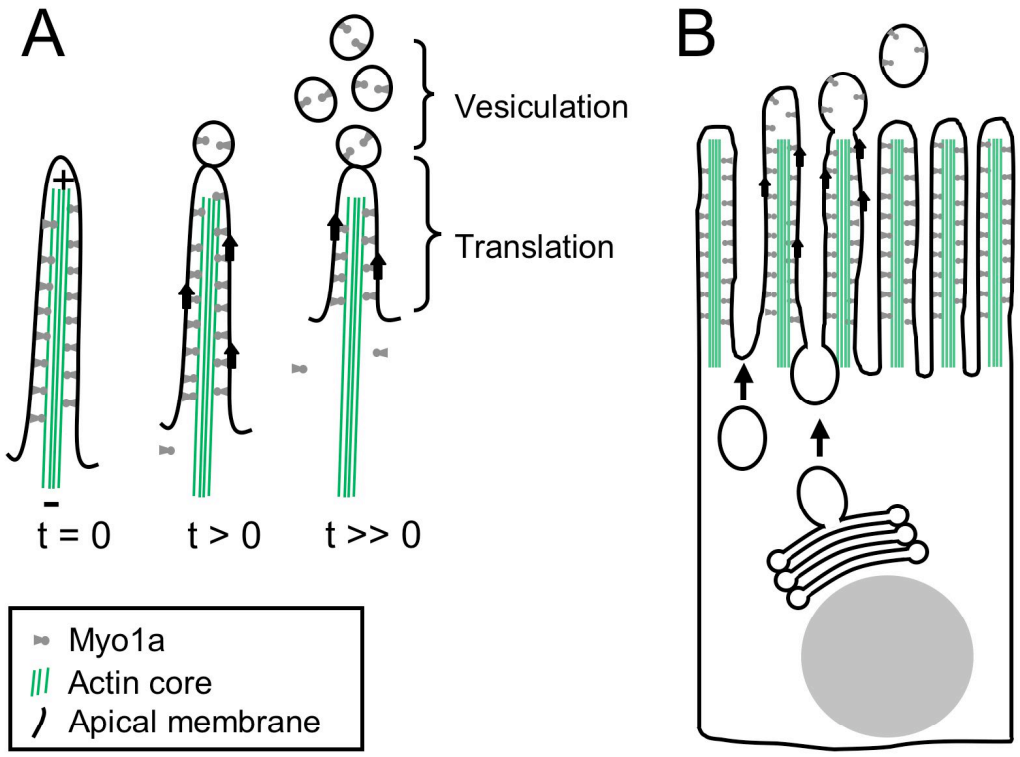

Figure 3-8. BB membrane shedding model.
(A) In isolated BBs, Myo1a motor activity powers the translation of apical membrane toward the actin bundle plus-end at the microvillus tip. Upon reaching the tip, membrane vesiculates and is shed from the BB. **(B)** In the context of an intact enterocyte, Myo1a-powered membrane translation may underlie the regulated turnover of BB membrane. New membrane is continually delivered to the terminal web, while older membrane is translated along microvillar actin bundles and eventually released from tips, into the intestinal lumen.

Myo1a was first visualized in microvilli in the form of lateral bridges (Mooseker and Tilney, 1975) at about the same time the early studies on BB contractility began (around 1976) (Rodewald et al., 1976). However, the motor properties of Myo1a were not discovered until the late 1980s (Mooseker and Coleman, 1989). We believe that this lag in the experimental timeline may explain why microvillar membrane translation and shedding were not described before this work. Interestingly, evidence of ATP-induced membrane vesiculation

consistent with that reported here can indeed be seen in ultramicrographs from studies on isolated BBs and microvilli performed before Myo1a was recognized as a bona fide motor protein (Howe and Mooseker, 1983; Rodewald et al., 1976; Verner and Bretscher, 1983).

Concluding remarks

The classic view of microvillar function suggests these structures serve to enhance the efficiency of nutrient uptake by amplifying the apical membrane surface area available for nutrient processing and absorption. The work presented here suggests that microvilli also function as actomyosin contractile arrays, allowing for the plus end–directed movement and shedding of BB membrane from microvillar tips. Because this process may have considerable implications with regard to gastrointestinal physiology, future studies will focus on investigating how Myo1a contributes to BB membrane shedding in vivo.

CHAPTER IV

THE ENTEROCYTE MICROVILLUS IS A VESICLE-GENERATING ORGANELLE

Russell E. McConnell[1], James N. Higginbotham[2], David A. Shifrin Jr.[1], David L. Tabb[4], Robert J. Coffey[1,2,3], and Matthew J. Tyska[1]

[1]Department of Cell and Developmental Biology, [2]Department of Medicine, [3]Department of Veterans Affairs Medical Center, [4]Department of Biomedical Informatics; Vanderbilt University Medical Center; Nashville, TN, 37232; USA

Keywords: myosin-1a, brush border, intestinal alkaline phosphatase, actin

To whom correspondence should be addressed:

Matthew J. Tyska, Ph.D.
Assistant Professor
Department of Cell and Developmental Biology
Vanderbilt University Medical Center
3130 Medical Research Building III
465 21st Avenue South
Nashville, TN 37232-8240
Phone: (615) 936-5461
Fax: (615) 936-5673
Email: matthew.tyska@vanderbilt.edu

Previously published as:
McConnell, R.E., J.N. Higginbotham, D.A. Shifrin, Jr., D.L. Tabb, R.J. Coffey, and M.J. Tyska. 2009. *The enterocyte microvillus is a vesicle-generating organelle.* J. Cell Biol. 185:1285-98.

Abstract

For decades, enterocyte brush border microvilli have been viewed as passive cytoskeletal scaffolds that serve to increase apical membrane surface area. However, recent studies revealed that in the *in vitro* context of isolated brush borders, myosin-1a powers the sliding of microvillar membrane along core actin bundles. This activity also leads to the "shedding" of small vesicles from microvillar tips, suggesting that microvilli may function as vesicle-generating organelles *in vivo*. Here we present data in support of this hypothesis, showing that enterocyte microvilli release unilamellar vesicles into the intestinal lumen; these vesicles retain the right-side-out orientation of microvillar membrane, contain catalytically active brush border enzymes, and are specifically enriched in intestinal alkaline phosphatase. Moreover, myosin-1a knockout mice demonstrate striking perturbations in vesicle production, clearly implicating this motor in the *in vivo* regulation of this novel activity. In combination, these data show that microvilli function as vesicle-generating organelles, which enable enterocytes to deploy catalytic activities into the intestinal lumen.

Introduction

The small intestinal epithelial cell (enterocyte) brush border is a highly ordered cellular specialization that functions as a primary site of nutrient processing and absorption as well as the major barrier to the resident intestinal microbiota and to

pathogens introduced into the gastrointestinal tract (Mooseker, 1985). The brush border of a single cell consists of thousands of tightly packed microvilli that extend off of the apical cell surface. Each microvillus consists of a cylindrical membrane protrusion (100-nm diameter x 1–2-μm long) that is supported by a polarized bundle of actin filaments oriented with plus ends extending into the tip (Mooseker and Tilney, 1975). These core bundles are held together with the cross-linking proteins villin, fimbrin, and espin (Revenu et al., 2004), which provide mechanical stability and regulate the dynamics of actin turnover (Loomis et al., 2003). The obvious structural consequence of this distinctive arrangement is that a brush border can accommodate 100-fold more membrane than a flat surface would afford; the coordinate functional consequence is an immense capacity for housing various membrane-bound transporters and channels that endow the brush border with its absorptive properties. Indeed, the functional significance of normal brush border structure is underscored by the fact that disruption of brush border membrane organization is associated with several pathological conditions, including microvillus inclusion disease (Cutz et al., 1989) and gluten-sensitive enteropathies such as Celiac Disease (Bailey et al., 1989; Iancu and Elian, 1976).

Within enterocyte microvilli, the plasma membrane is connected to the core actin bundle by the motor protein myosin-1a (myo1a) (Mooseker and Coleman, 1989; Mooseker and Tilney, 1975). As alluded to in the previous paragraph, enterocyte microvilli have historically been viewed as passive cytoskeletal scaffolds that increase apical membrane surface area, thereby

enhancing the nutrient processing and absorptive capacity of the intestinal epithelium (Brown, 1962). However, recent findings have challenged this model by demonstrating that in isolated brush borders, myo1a is able to propel microvillar membrane over core actin bundles (McConnell and Tyska, 2007). This movement results in the shedding of membrane from microvillar tips in the form of small (100-nm diameter) unilamellar vesicles, raising the intriguing possibility that microvilli might function as active, vesicle-generating organelles. Because the brush border is positioned at the enterocyte–lumen interface, the shedding of microvillar membrane could represent an important aspect of enterocyte functions that involve communicating with and/or conditioning the lumenal environment (Bates et al., 2007; Goldberg et al., 2008; Jacobs, 1983).

As our initial experiments were limited to in vitro observations using isolated brush borders (McConnell and Tyska, 2007), the possibility that microvilli function as vesicle-generating organelles has not been explored. Thus, the goal of this study was to combine light microscopy and EM with biochemical and proteomic approaches to investigate this hypothesis. Our findings clearly show that native microvilli are capable of releasing vesicles from their distal tips in vivo. The resulting vesicles contain several catalytically active enzymes normally associated with the brush border but are specifically enriched in intestinal alkaline phosphatase (IAP). In a manner consistent with our previously published in vitro data (McConnell and Tyska, 2007), we find that myo1a knockout (KO) mice demonstrate marked defects in vesicle production. Based on these data, we propose that enterocyte microvilli function as active vesicle-generating

organelles. This novel aspect of epithelial cell biology may enable enterocytes to distribute specific enzyme activities into the intestinal lumen to serve in nutrient processing and/or host defense.

Results

Bulbous protrusions of apical membrane are found at microvillar tips in vivo

Although our previous experiments indicate that microvilli hold the potential to produce vesicles (McConnell and Tyska, 2007), these experiments were performed with isolated brush borders. If microvilli do produce vesicles in vivo, one would expect to observe morphological evidence of this process at the level of individual microvilli in the context of native intestinal tissue samples. To test this prediction, we examined rat small intestine using scanning EM (SEM), an approach well suited for the visualization of cell surface features. High magnification (50,000x) observations in ad libitum–fed adult rat duodenum revealed the presence of bulbous membrane protrusions at the distal tips of microvilli with a mean diameter of 102.5 ± 13.1 nm (Fig. 4-1, A and B). Although not present on the tip of every microvillus, these protrusions or "bulbs" appeared to be ubiquitous, as they were present on the surface of enterocytes along the length of a given villus. Apical membrane bulbs were also observed in confocal micrographs of intestinal frozen sections fluorescently labeled with Con A and phalloidin to mark the apical membrane and actin filaments, respectively (Fig. 4-1, C and D). These images clearly show membrane protruding from enterocytes into what would be lumenal space (Fig. 4-1 D, arrowheads). Importantly, bulbs

were devoid of phalloidin signal, ruling out the possibility that these structures simply represent microvilli of above average length.

The membrane bulbs imaged in both SEM and confocal micrographs (Fig. 4-1, B [red circles] and D [arrowheads]) bear a striking resemblance to the vesiculating membrane observed at microvillar tips of isolated brush borders after ATP exposure (McConnell and Tyska, 2007). Thus, distal tip bulbs may represent structural intermediates in the process of microvillar membrane shedding.

Vesicles containing microvillar membrane markers are found in the intestinal lumen

Vesicles released from the tips of microvilli in vivo should accumulate in the intestinal lumen. To determine whether such vesicles are present, full lengths of small intestine were dissected out of adult rats and flushed with saline; the resulting lumen wash was then fractionated using differential and gradient centrifugation. Gradient fractions were assayed for the presence of enterocyte-derived vesicles using negative-stain transmission EM (TEM) and Western blot analysis using antibodies directed against microvillar membrane components (Fig. 4-2). Gradient fraction 3, which included the 16–25% sucrose interface, was highly enriched in unilamellar vesicles with a size comparable with the diameter of microvilli (100 nm), as observed using negative stain and ultrathin section TEM (Fig. 4-2, B and C). Western blotting revealed that this lumenal vesicle (LV) fraction contains several integral membrane proteins that are expressed in enterocytes and found in the brush border, including maltase glucoamylase (MGAM), lactase-phlorizin hydrolase (LPH), sucrase isomaltase (SI), dipeptidyl peptidase IV (DPPIV), and IAP (Fig. 4-2 A). Importantly, actin was not detectable

in any of the gradient fractions, indicating that vesicles at the 16–25% interface are not likely the result of microvillar/brush border fragmentation. These data show that small vesicles, which may be derived from the microvillar membrane, are in fact found in the intestinal lumen.

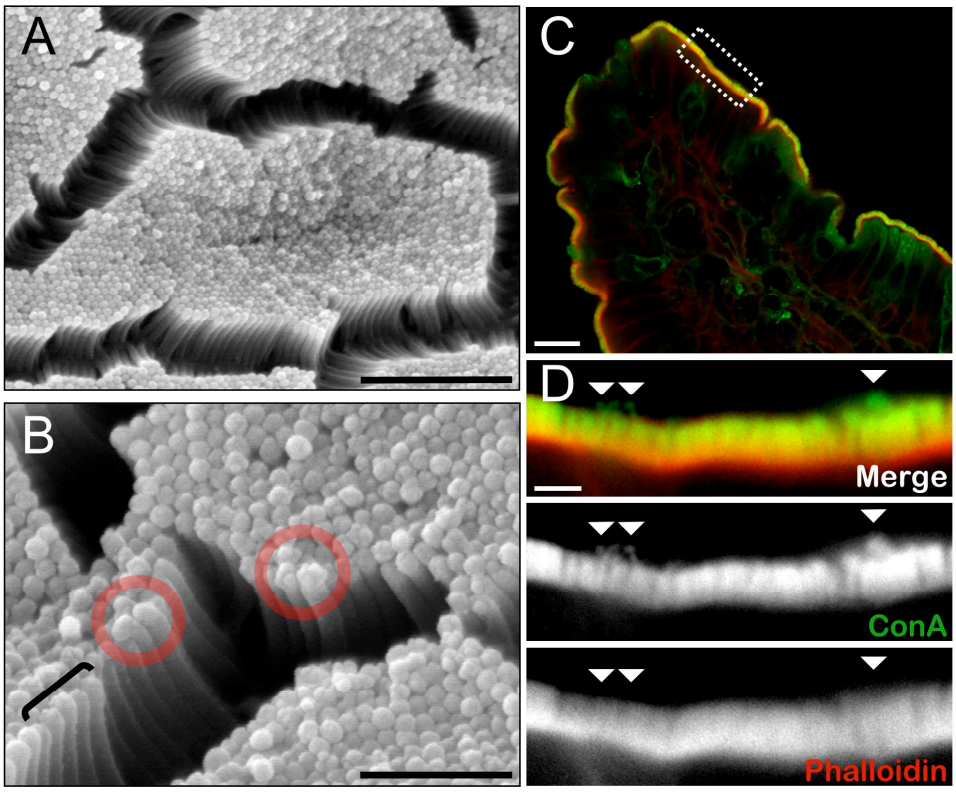

Figure 4-1. Bulbous membrane protrusions are observed at microvillar tips.
(A) SEM micrograph of the duodenum lumenal surface shows the presence of membrane extensions at the tips of large numbers of enterocyte microvilli. Membrane bulbs displayed a mean diameter of 102.5 ± 13.1 nm (*n* = 100). Bar, 1.6 µm. **(B)** A higher magnification view of the enterocyte apical surface reveals that some microvilli demonstrate characteristically regular height and tip diameter (bracket), whereas others have enlarged or irregular tips (red circles). Bar, 0.6 µm. **(C)** Low magnification confocal micrograph of a section through a small intestine villus labeled with fluorescent conjugates of the lectin Alexa Fluor 488–Con A (green) and the filamentous actin–binding protein Alexa Fluor 633–phalloidin (red) to mark membranes and actin, respectively. Enterocyte brush borders line the lumenal surface of the villus and are visualized as the strongly labeled yellow band at the villus perimeter. Bar, 10 µm. **(D)** A high magnification view of the boxed area in C is shown. Small membrane bulbs protruding from the tips of microvilli can be seen (arrowheads). Note that the membrane bulbs do not contain actin filaments. Bar, 2 µm.

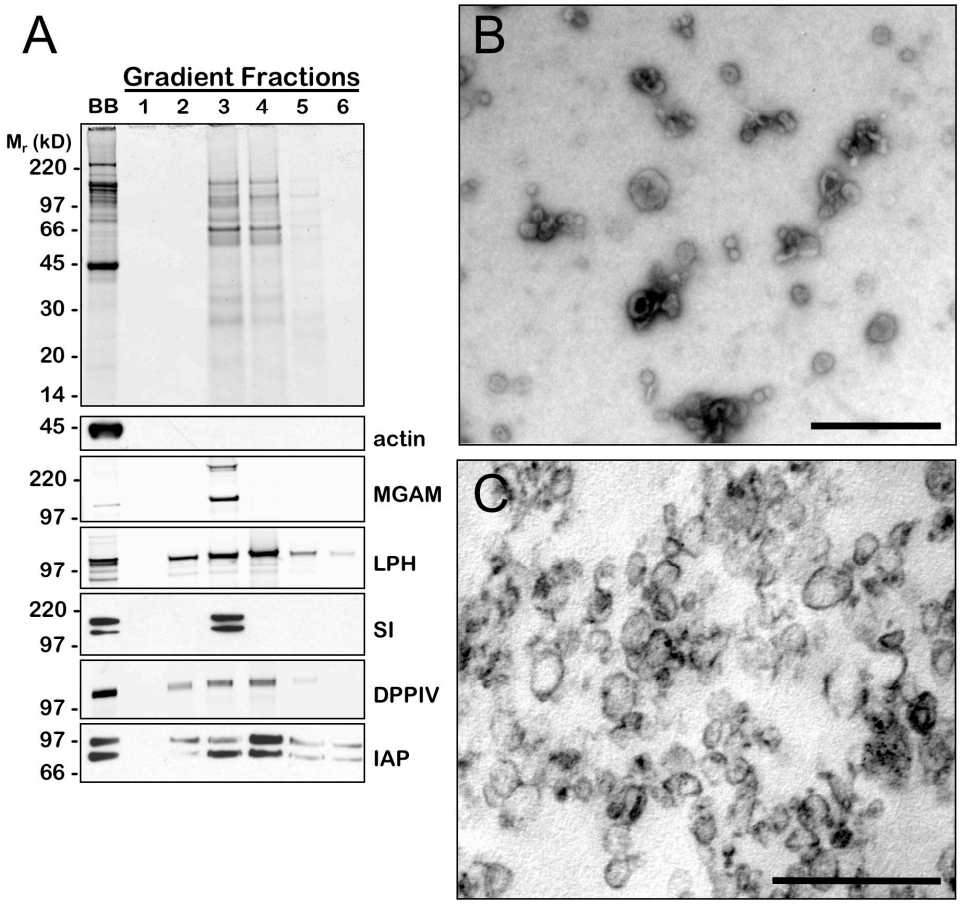

Figure 4-2. Isolation of vesicles from the intestinal lumen.
(A) Lumenal contents from rat small intestine were fractionated using differential centrifugation (see Materials and methods); the resulting 100,000 *g* pellet was resuspended and loaded onto a discontinuous sucrose gradient. A Coomassie blue–stained gel of the gradient fractions shows that most of the protein is found in fractions 3 and 4. Western blot analysis reveals that fraction 3 contains several membrane proteins that are found at high levels in the enterocyte microvillar membrane (MGAM, LPH, SI, DPPIV, and IAP) and does not have detectable levels of actin. **(B)** Negative-stain TEM of fraction 3 shows the presence of membrane structures in the intestine lumenal contents that are similar in size to the membrane accumulations observed at the tips of microvilli. **(C)** Ultrathin sections of fraction 3 viewed by TEM clearly show that the majority of vesicles present in this fraction are unilamellar. Bars, 0.5 μm.

LV membranes are oriented right side out

Based on our in vitro experiments, vesicles released during microvillar membrane shedding are expected to retain the orientation of the native microvillar membrane (McConnell and Tyska, 2007). To determine whether LVs are oriented "right side out," vesicles were mixed with papain-conjugated beads to cleave exposed proteins from the vesicle surface (Maestracci, 1976). After papain treatment, LVs were centrifuged (100,000 *g*) and the pellet analyzed by Western blotting. Increasing concentrations of papain resulted in progressively more protein cleavage; at the highest papain concentration, IAP and SI were completely lost from the LV pellet (Fig. 4-3 A). Similarly, phosphatidylinositol-specific PLC (PI-PLC) released the glycosylphosphatidylinositol-anchored protein IAP from the LV pellet into the supernatant without affecting the transmembrane protein SI (Fig. 4-3 B). These data show that LV membrane proteins are surface exposed and suggest that LVs are right side out; i.e., LV membrane has the same orientation as microvillar membrane.

LV-associated enzymes are catalytically active

Given the right side out orientation of vesicles in the LV fraction, component enzymes should have access to substrates present in the lumen and may therefore exhibit catalytic activities. We investigated the presence of enzyme activities in the LV fraction using substrates specific to common brush border hydrolases. Strikingly, LVs possessed activities comparable with brush border controls with nearly identical IAP and aminopeptidase activities in assays loaded

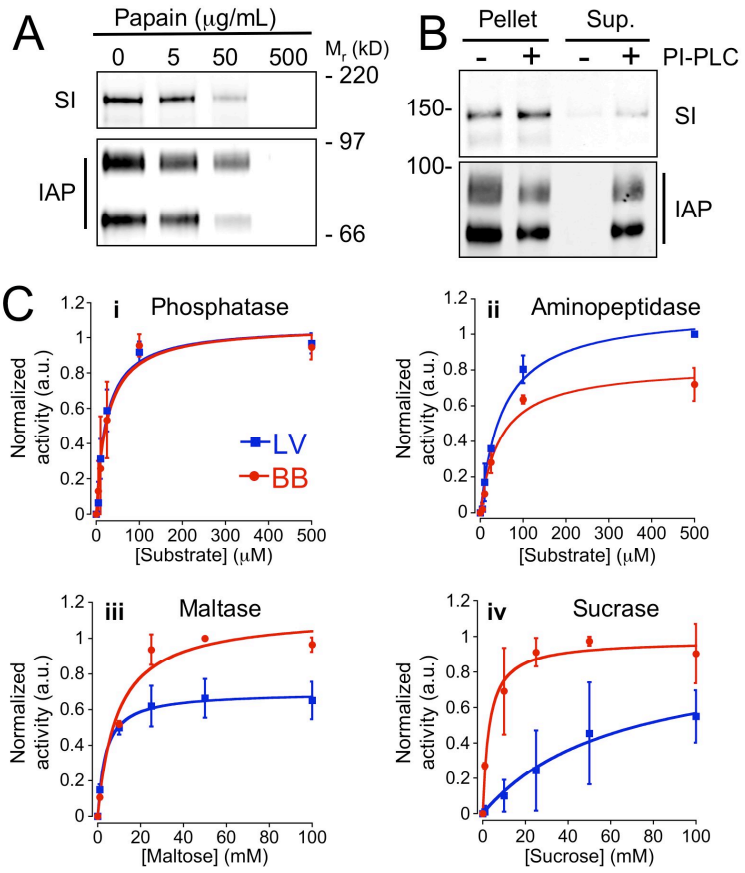

Figure 4-3. LVs are oriented right side out and exhibit catalytic activity.
(A) Intact LVs were incubated with increasing concentrations of papain-conjugated beads, the beads were removed with centrifugation (500 *g*), and the supernatant was centrifuged (100,000 *g*) to pellet LVs. Western blot analysis of the 100,000 *g* pellet shows that both IAP and SI are cleaved from LVs by papain, with neither protein being detectable in the 100,000 *g* pellet at the highest papain concentration. **(B)** LVs incubated with PI-PLC for 15 min at 30°C were pelleted with ultracentrifugation (100,000 *g*), and membrane protein distributions were examined by Western blotting. In control samples (–), IAP and SI were found entirely in the pellet fraction. PI-PLC treatment (+) released approximately half of the IAP from the pellet into the supernatant. The transmembrane protein SI was unaffected by PI-PLC treatment, remaining in the pellet in both control (–) and PI-PLC–treated (+) samples. **(C)** The enzyme activities of intact LVs (25 μg; blue squares) were compared with isolated brush borders (25 μg; red circles) using the fluorescent substrates 4-methylumbelliferyl phosphate (i) and *H*-Leu-7-amino-4-methylcoumarin (ii) to measure phosphatase and aminopeptidase activities, respectively. To assess disaccharidase activities, samples were incubated with maltose (iii) and sucrose (iv), and liberated glucose was measured using a hexokinase assay (Sigma-Aldrich). LVs demonstrated robust phosphatase and aminopeptidase activities (i and ii) but possessed significantly less maltase (iii) and sucrase (iv) activities ($P < 0.05$). Data are presented as mean ± standard error of the mean. Error bars show fits to a Michaelis–Menten model: normalized activity = $(V_{Max} \times [substrate])/(K_M + [substrate])$.

for equal total protein (Fig. 4-3 C, i and ii). Although LVs did possess disaccharidase activities, these were significantly lower than those of isolated brush borders (Fig. 4-3 C, iii and iv). These results demonstrate that LV-associated enzymes are catalytically active and suggest that LV production may be a means of distributing specific enzymatic activities into the intestinal lumen.

LVs are specifically enriched in IAP

To further develop insight into LV function, we sought to determine which LV-associated proteins were enriched or depleted relative to the composition of whole microvillar membrane. When detergent-extracted LV and microvillar membranes were separated using 30% iodixanol gradients (Optiprep; Sigma-Aldrich), the resulting fractions demonstrated comparable cholesterol distributions (Fig. 4-4, A and B). Western blot analysis of gradient fractions revealed that LV and microvillar membrane proteins undergo similar partitioning between detergent-resistant and detergent-soluble membrane fractions (Fig. 4-4 D). Although LVs contained many of the same proteins as microvillar membrane, they were depleted in SI, LPH, and MGAM. In contrast, LVs were enriched in a prominent doublet running between 50 and 100 kD in the lowest density fraction (Fig. 4-4 D, fraction 1). To identify these two major components, we excised both bands, trypsinized the samples, and performed liquid chromatography/mass spectrometry (MS) on the resulting peptides. Our results show with high confidence that these bands represent the two distinct forms of IAP expressed in the rat gastrointestinal tract (51% coverage of IAP1 and 30% coverage for IAP2)

(Xie and Alpers, 2000). Western blot analysis and enzyme activity assays confirmed that IAP is significantly enriched in the LV fraction compared with microvillar membranes (Fig. 4-4, C and D). Thus, although LVs and microvillar membranes share several common components, these data indicate that IAP is a principal cargo of LVs.

Because LVs are highly enriched in IAP (Fig. 4-4 D), one might expect to find that IAP is also enriched in the aforementioned distal tip membrane bulbs (Fig. 4-1). Indeed, small intestine frozen sections labeled with an antibody directed against IAP show intense labeling at the distal microvillus tips (Fig. 4-4 E). Consistent with the Western blot (Fig. 4-4 D) results, the type II transmembrane protein SI was also present in microvillar membrane bulbs but did not exhibit the enrichment observed for IAP (Fig. 4-4 E). The enrichment of IAP at microvillar tips (Fig. 4-4 E)is consistent with the hypothesis that IAP-enriched LVs isolated from the intestinal lumen (Fig. 4-2) are derived from the enterocyte brush border.

IAP-enriched LVs are derived from enterocyte microvillar membrane

The morphological heterogeneity of vesicles in the LV fraction (Fig. 4-2 B) suggests that this material may represent a mixture of membranes from multiple cellular sources. However, we were interested in determining whether LVs enriched in IAP were derived specifically from enterocyte microvilli. To this end, we used a novel high performance flow cytometry approach called fluorescence-activated vesicle sorting (FAVS) to isolate only IAP-enriched vesicles (Cao et al., 2008). Our goal was to create a purified pool of IAP-enriched vesicles that could

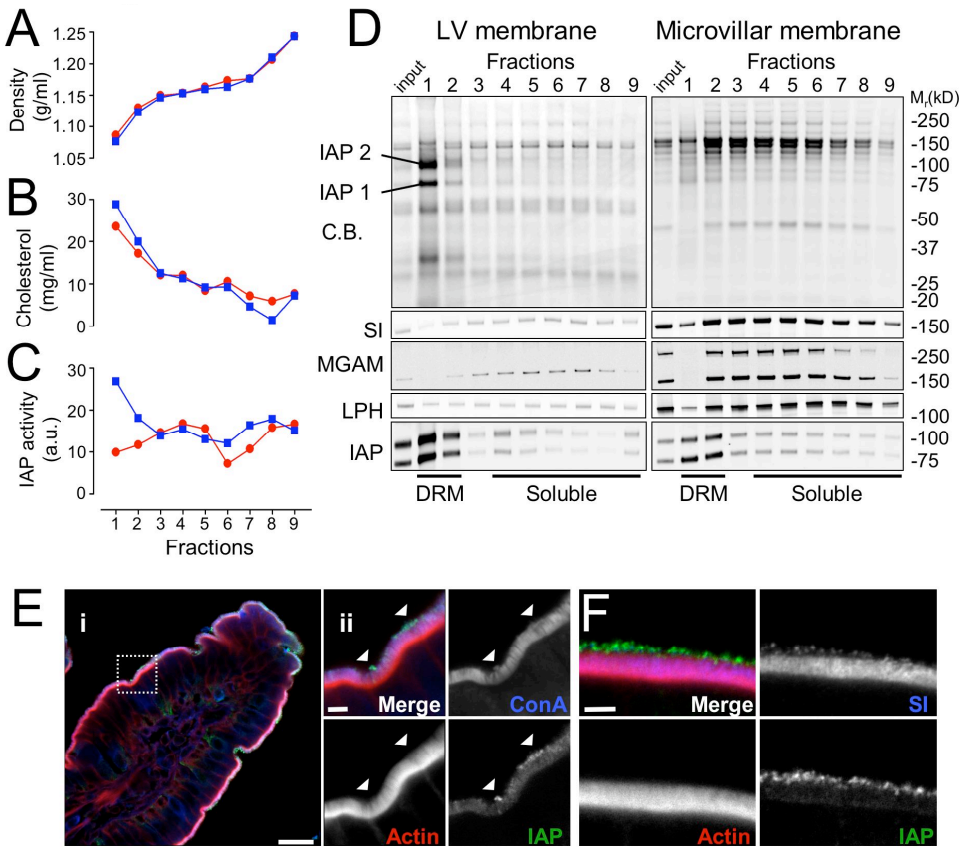

Figure 4-4. LVs are specifically enriched in IAP.
(A) LVs and microvillar membrane were extracted with 1% NP-40 on ice and loaded onto self-forming Optiprep density gradients. Density profiles of 30% Optiprep density gradients are shown. **(B)** Optiprep gradient fractions of LV and microvillar membrane were analyzed using an Amplex Red Cholesterol Assay kit (Invitrogen). Cholesterol from both samples distributed similarly, showing obvious enrichment in the low density fractions (fractions 1 and 2). **(C)** IAP enzyme activity was assayed using the quenched fluorescent substrate phenylumbelliferyl phosphate. LV Optiprep gradient fraction 1 demonstrated the highest phosphatase activity, with considerably less activity detected in the microvillar membrane fractions. (A–C) Blue squares, LVs; red circles, microvillar membrane. **(D)** Optiprep gradient fractions were separated using SDS-PAGE. Coomassie blue (CB)–stained gels show the distribution of LV and microvillar membrane proteins between detergent-resistant membrane (DRM) and detergent-soluble fractions (loaded for equal volume). The two prominent bands observed in LV fraction 1 were excised and identified by MS as the two isoforms of IAP found in rat. Western blot analysis confirmed the enrichment of IAP in this fraction, while demonstrating that the enterocyte membrane proteins SI, MGAM, and LPH were depleted in LVs relative to microvillar membrane. **(E)** Confocal micrographs of sections through small intestine villi labeled with Alexa Fluor 488–Con A (blue), Alexa Fluor 633–phalloidin (red), and an antibody directed against IAP (Alexa Fluor 568; green). (ii) A high magnification view of the boxed area in i shows that Con A–labeled membrane extensions are enriched in IAP and devoid of actin staining (arrowheads). IAP enrichment was observed in membrane extensions found at the tips of microvilli in every villus examined (n = 30). Bars: (i) 20 μm; (ii) 2 μm. **(F)** Confocal micrographs of sections through small intestine villi labeled with Alexa Fluor 633–phalloidin (red) and antibodies directed against IAP (green) and SI (blue). The obvious enrichment of IAP at the microvillus tip is in stark contrast to SI, which localizes predominantly along the actin-supported length of the microvillus. Bar, 2 μm.

serve as input for proteomic analysis; the resulting dataset would provide definitive information on the origin of LVs. Vesicles in fraction 3 (Fig. 4-2) were labeled with the fluorescent lipophilic dye DiD (1,1'-dioctadecyl-3,3,3',3'-tetramethylindodicarbocyanine perchlorate) and a polyclonal antibody directed against IAP (Sigma-Aldrich; detected with an Alexa Fluor 488–conjugated secondary antibody). By comparing the light-scattering and fluorescence signal characteristics of LVs with those of reference beads, we were able to isolate particles that were (a) double positive for both DiD and IAP, (b) single vesicles (i.e., not aggregates), and (c) in the expected size range of 100 nm (Fig. 4-5; see Materials and methods). Our ability to isolate particles meeting these criteria was confirmed by postsorting flow analysis (Fig. 4-5 B; note the wide dispersion of the input material relative to the tight grouping of the postsort particles within the established gates). Selection of particles of the appropriate size and composition was validated by negative-stain TEM and Western blot analysis (Fig. 4-5).

Sorted vesicles had a slightly larger mean diameter (90 nm) and fell within a range of 30–170 nm, completely lacking the large (>400-nm diameter) particles observed in the input material (Fig. 4-5). Additionally, postsort LVs were highly enriched in IAP (the sorting marker) and modestly enriched in other microvillar membrane proteins such as SI, DPPIV, and LPH (Fig. 4-5 D). The uniform appearance of vesicles and accompanying enrichment in microvillar membrane markers confirmed the utility of FAVS for purifying IAP-enriched LVs.

After validating the FAVS purification procedure, sorted LVs were concentrated by ultracentrifugation and subjected to proteomic analysis. Peptide

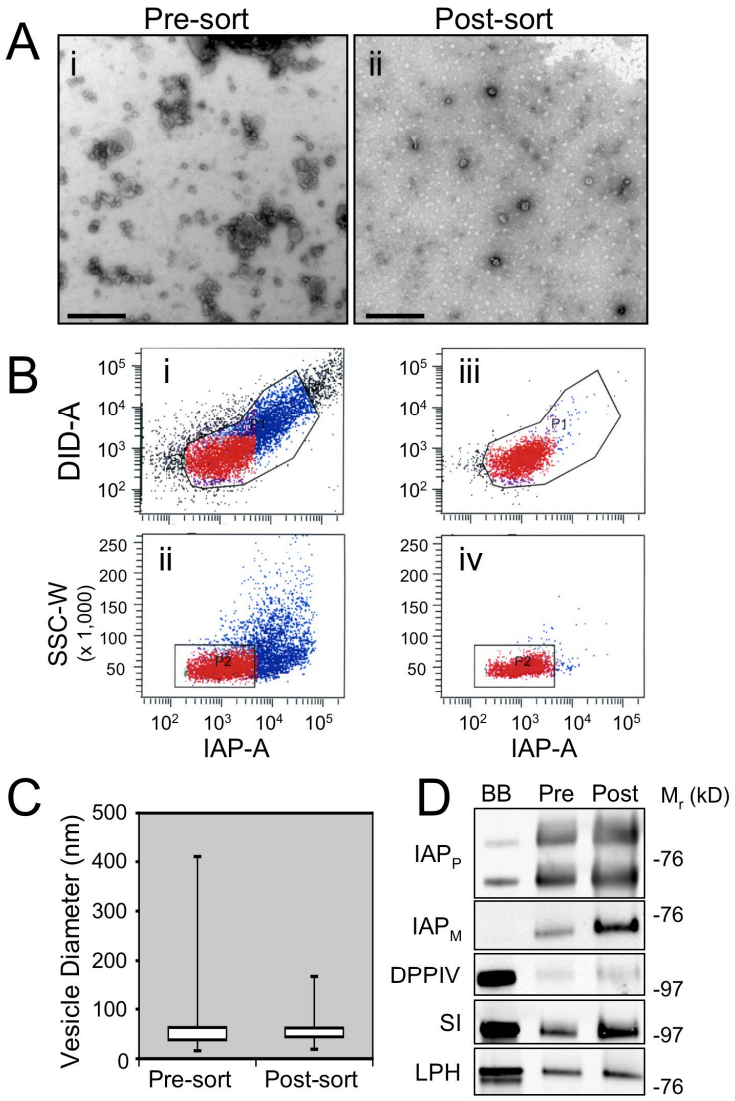

Figure 4-5. Purification of IAP-enriched LVs by FAVS.
(A) Negative-stain TEM of vesicles present in sucrose gradient fraction 3. The considerable size variation observed before FAVS (i) is notably decreased after sorting (ii). Bars, 0.5 μm. **(B)** Fraction 3 vesicles were labeled with the lipophilic dye DiD and an Alexa Fluor 488 antibody to detect IAP as outlined in Materials and methods. Light-scattering properties were used to eliminate large particles or aggregates. Particles within established gates (black outlines; red denotes particles included in all gates) were isolated for further analysis, whereas particles outside of the fluorescence and light-scattering (side-scattered light [SSC]) gates were excluded (colored black and blue, respectively). Plots of the fluorescence and light-scattering properties of vesicles before (i and ii) and after (iii and iv) sorting show that particles falling within established gates were physically isolated; compare the tight grouping of the FAVS-purified LVs (iii and iv) with the wide dispersion of unsorted vesicles (i and ii). **(C)** Box and whisker plot of vesicle diameters measured from negative-stain TEM micrographs. The diameters of vesicles before (*n* = 1219) and after (*n* = 372) FAVS were measured from electron micrographs of negatively stained samples. Postsort vesicles displayed less variability in their size with no vesicles >170 nm, which is in contrast with the presort vesicles that regularly possessed membrane particles as large as 400 nm. **(D)** Samples of brush borders (BB) and pre- and post-FAVS–purified LVs were analyzed by Western blotting (loaded for equal total protein). FAVS-purified LVs show a clear enrichment in IAP when detected using either a polyclonal (IAP_P) or monoclonal (IAP_M) antibody. DPPIV, SI, and LPH are found at lower levels in LVs than in the brush border but all show modest enrichment after FAVS purification.

spectra were analyzed and assigned to protein identifications using MyriMatch software (Tabb et al., 2007); general characterization based on function and localization of identified proteins was determined using WebGestalt (version 2.0) (Zhang et al., 2005)and manually cross-checked against the National Center for Biotechnology Information protein database (http://www.ncbi.nlm.nih.gov/sites/entrez?db=Protein). Strikingly, several of the identified LV cargos are only expressed in enterocytes where they are known to localize to the microvillus; these include the actin-bundling protein ezrin, the carbohydrate-binding protein galectin-4, and a variety of well-characterized brush border hydrolases (Table I). Hydrolases made up the largest class of cargos and included peptidases, glycosidases, lipases, and phosphatases (Table I). LVs also contained several proteins that have been implicated in immunological function, inflammatory response, or are misregulated in cancer; prominent examples include the polymeric Ig receptor (Murthy et al., 2006), several annexins (Gerke et al., 2005), meprin (Lottaz et al., 2007), syncollin (Tan and Hooi, 2000), alkaline sphingomyelinase (Hertervig et al., 1997; Sakata et al., 2007), and ceramidase (Teichgraber et al., 2008). Additional LV cargoes included proteins with established roles in modifying the chemistry or curvature of cellular membranes such as annexin A13b (Gerke et al., 2005) and secreted PLA2 (Table I) (Staneva et al., 2004). The identification of numerous membrane proteins that are components specifically found in the enterocyte brush border clearly shows that IAP-enriched vesicles are derived from the microvillar membrane.

Myo1a KO mice demonstrate defects in IAP-enriched LV production

Given that our structural, biochemical, and proteomic data all indicate that LVs are released from brush border microvilli, we sought to determine whether LV production was disrupted in the absence of the major microvillar motor protein, myo1a. Myo1a is likely to play a role in LV production in vivo, as our previous experiments have revealed that this motor is required to power the release of vesicles from microvillar tips in isolated brush borders (McConnell and Tyska, 2007). When KO lumen washes were processed to isolate LVs, we were surprised to find that even in the absence of myo1a, a significant amount of membranous material was present in the LV fraction. However, when we examined this material by negative-stain TEM, we observed that KO vesicles are significantly larger than those isolated from wild-type (WT) controls (Fig. 4-6). An increase in vesicle size was confirmed using analytical flow cytometry (vesicles labeled as in the aforementioned FAVS purification protocol) in which DiD fluorescence provides a readout on the relative amount of membrane present in each particle. Of the 10,000 WT LVs analyzed, we observed a nearly linear relationship between IAP content and vesicle size (DiD signal) with >92% of the vesicles grouping into a tightly defined gate (Fig. 4-6 B, blue). However, when KO LVs were processed identically, we found that nearly half of the KO vesicles fell outside of this area (48%; Fig. 4-6 B, red). This analysis reveals that KO vesicles contain more lipid (per particle) on average relative to WT (i.e., KO LVs are

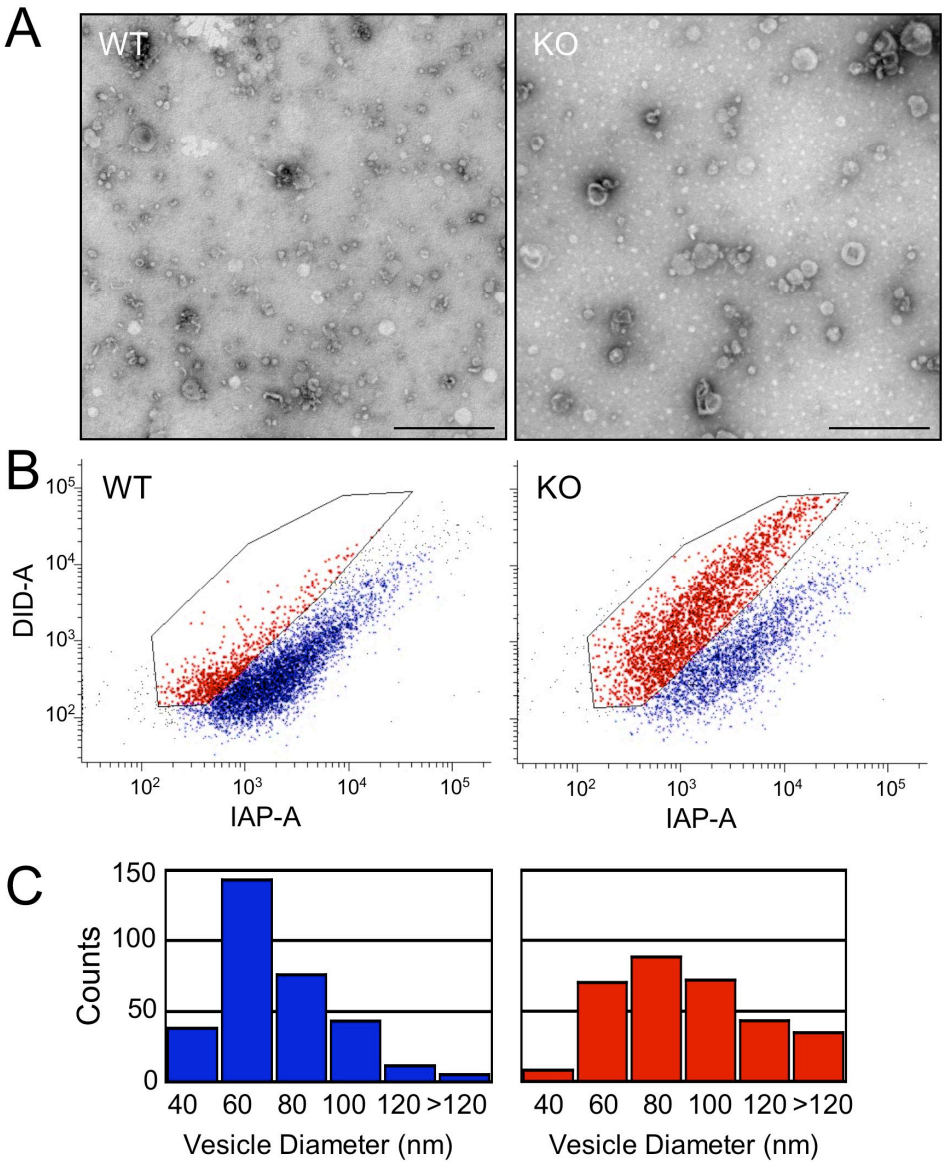

Figure 4-6. LVs isolated from myo1a KO mice exhibit abnormal morphology.
(A) Negative-stain TEM clearly shows that LVs isolated from myo1a KO mice are much larger than WT controls. Bars, 0.5 µm. **(B)** Flow cytometric analysis of WT and KO LVs fluorescently labeled with the membrane dye DiD and an antibody directed against IAP. KO LVs had much higher DiD fluorescence per particle, suggesting that these particles had more membrane; i.e., vesicles are larger. This larger size is clearly visualized by the shift up the y axis; compare the outlined areas in WT and KO (included particles highlighted in red). Although only 12% of WT particles fall into this gate, nearly half (48%) of the particles analyzed from KO mice demonstrated increased DiD fluorescence. 10,000 particles were analyzed for each condition. **(C)** LVs isolated from myo1a KO mice (red bars) are significantly larger than WT LVs (blue bars). Negative-stain TEM images of WT and KO LVs were used to quantify vesicle diameters (n = 316 per condition). Although vesicle size distributions overlapped, WT LV diameters clustered around a mean value of 70 nm. KO LVs showed a much broader size distribution, with many of the LVs displaying diameters well over 120 nm. These larger vesicle sizes were extremely rare in preparations of WT LVs.

larger) and further suggests that the IAP/lipid ratio is lower than normal in the absence of myo1a.

To further characterize defects in the production of myo1a KO LVs, we analyzed the density of WT and KO vesicles in 100,000 *g* lumen wash pellets using self-forming Optiprep density gradients. With this approach, WT vesicles typically demonstrated peak IAP enrichment in the first gradient fraction (lowest density, 1.05 g/ml); KO samples lacked the enrichment of IAP in the first fraction, instead displaying an even distribution across the entire gradient (Fig. 4-7 A). These results are consistent with the aforementioned flow cytometry data described; both assays suggest that the effective IAP concentration in KO vesicles is reduced. To determine whether vesicle composition was altered in general, WT and KO vesicles from sucrose gradient fraction 3 were analyzed by Western blotting (loaded for equal total protein). We found that although IAP levels appear comparable, KO LVs possess abnormally high levels of other brush border membrane proteins such as MGAM, SI, and LPH when compared with WT (Fig. 4-7 B). Intriguingly, we observed a corresponding decrease in the levels of these enzymes in KO brush borders (Fig. 4-7 B). When the disaccharidase activities of equivalent amounts of LVs and brush borders were compared (equal total protein), we observed that both sucrase and maltase activities were high in WT brush borders with minimal activity present in WT LVs. However, KO LVs showed high disaccharidase activities with a corresponding decrease in these activities in KO brush borders (Fig. 4-7 C).

Given the high expression level of myo1a in the enterocyte and its specific targeting to microvilli, the data derived from experiments with myo1a KO mice provide strong evidence implicating the microvillus as the source of LVs. Moreover, the redistribution of components from the brush border into LVs in KO animals indicates that myo1a is critical for the production of vesicles that contain a normal complement of enzymes and are specifically enriched in IAP.

Figure 4-7. LVs isolated from myo1a KO mice exhibit defects in protein composition.

(A) To analyze LV density, lumen wash material from WT and KO mice was fractionated by differential centrifugation as described in Materials and methods. The 100,000 *g* pellets were resuspended in PBS, loaded onto 20% self-forming Optiprep gradients, and centrifuged at 200,000 *g* for 2 h. Gradients were split into 10 equal-volume fractions; dashed lines denote fraction density. WT LVs demonstrate clear enrichment of IAP in low density fractions (fractions 1 and 2); this enrichment is completely lacking in the KO LVs. IAP enrichment was calculated by normalizing IAP levels (Western blot densitometry) against total protein for each fraction. **(B)** Polyacrylamide gel of LV and brush border (BB) samples isolated from WT and myo1a KO mice stained with Coomassie blue (CB). The increased staining in the KO LV sample in the high molecular mass range (76–225 kD) was observed in multiple experiments. When these samples were analyzed by Western blotting (WB) using antibodies directed against brush border membrane proteins found in this size range, we observed that several integral membrane proteins normally found at low levels in WT LVs are present at significantly higher levels in KO LVs (e.g., MGAM, SI, and LPH). **(C)** Sucrase and maltase activities of LV and brush border samples isolated from WT and KO mice were assayed by measuring glucose liberated from sucrose and maltose, respectively (12.5 µg protein per condition). Both sucrase and maltase activities distributed differently, with KO LVs showing higher disaccharidase activities than WT LVs, whereas KO brush borders showed a corresponding decrease in these activities relative to WT brush borders. Values are given as millimoles of sugar hydrolyzed per hour per microgram of protein (mmol h^{-1} μg^{-1}). Sucrase: WT LV, 0.05 ± 0.21; KO LV, 0.94 ± 0.18; WT brush border, 1.16 ± 0.19; KO brush border, 1.14 ± 0.13. Maltase: WT LV, 2.97 ± 0.29; KO LV, 9.76 ± 0.52; WT brush border, 9.4 ± 0.19; KO brush border, 7.55 ± 0.15. Conditions were considered statistically significant if $P < 0.05$ (denoted by an asterisk).

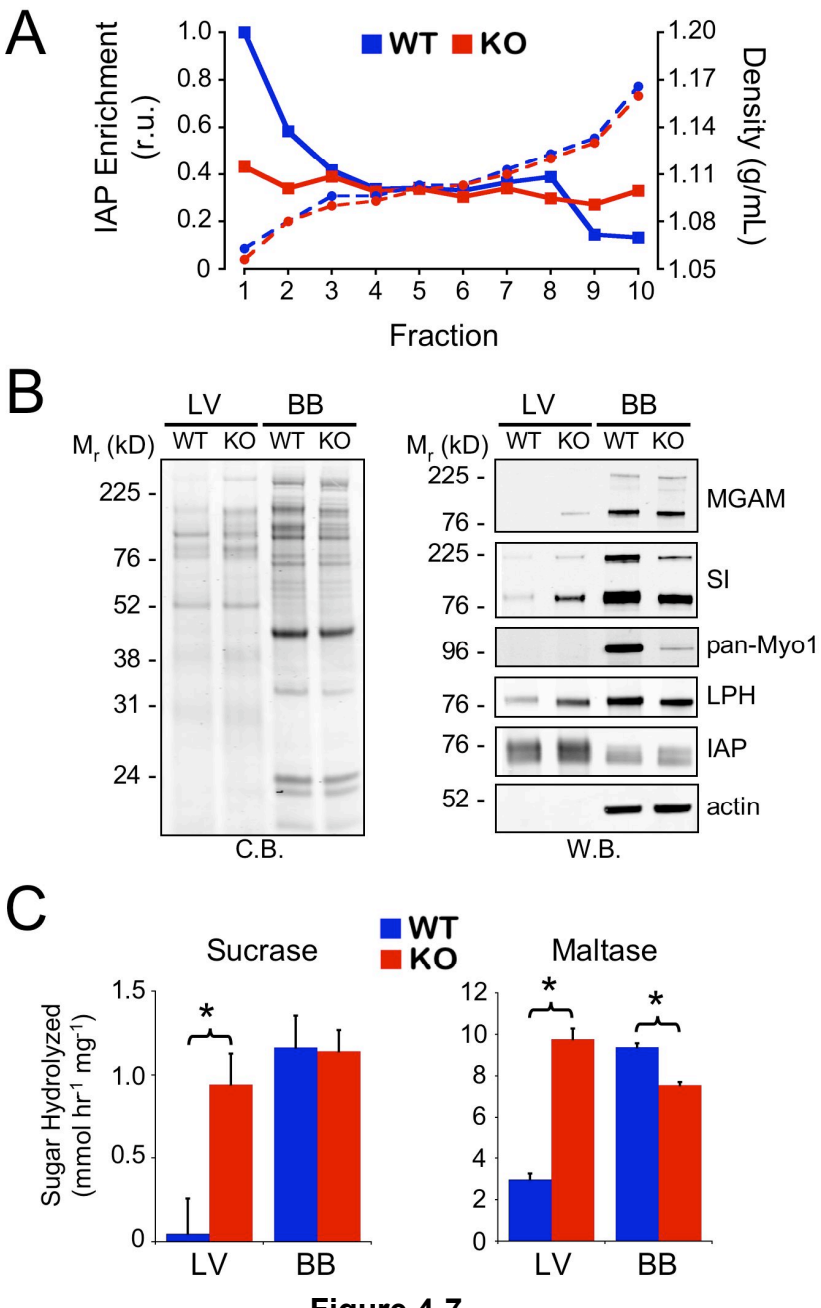
A
IAP Enrichment (r.u.)
Density (g/mL)
WT
KO
Fraction
B
LV
BB
WT KO WT KO
Mr (kD)
225 -
76 -
52 -
38 -
31 -
24 -
C.B.
MGAM
SI
pan-Myo1
LPH
IAP
actin
W.B.
C
Sucrase
Maltase
Sugar Hydrolyzed (mmol hr-1 mg-1)
LV
BB

Figure 4-7.

Discussion

Enterocyte microvilli function as vesicle-generating organelles

Previous studies have reported the presence of vesicles in the intestinal lumen (Beaudoin and Grondin, 1991; Eliakim et al., 1989; Halbhuber et al., 1994), although their function, origin, and mechanism of formation have not been elucidated. These studies, in combination with recent in vitro studies conducted in our laboratory(McConnell and Tyska, 2007), led us to hypothesize that enterocyte microvilli could serve as the source of these membranes by releasing vesicles laden with brush border enzymes from their distal tips. In this study, we present multiple lines of evidence in support of this model: (a) morphological experiments of native enterocytes clearly show that apical membrane forms bulbous protrusions at microvillar tips, (b) EM and biochemical analysis of intestinal lumen wash reveals that this material contains vesicles with the expected diameter and orientation (90 nm; right side out) for membranes released from microvillar tips, (c) LVs and membrane bulbs at the tips of microvilli are specifically enriched in IAP, (d) proteomic analysis of purified, flow-sorted LVs confirms that these vesicles contain an array of catalytically active enzymes (IAP, SI, MGAM, and aminopeptidase N) that are specific markers for the enterocyte microvillar membrane, and (e) the absence of myo1a causes defects in the structure and composition of both the enterocyte brush border (Tyska et al., 2005) and LVs (Fig.s 4-6 and 4-7). Together, these data indicate that microvilli play a role beyond that of passively scaffolding apical membrane by functioning as active vesicle-generating organelles.

Myo1a is required for proper LV production

Within the intestinal tract, myo1a is expressed only in enterocytes and localizes exclusively to brush border microvilli (Bikle et al., 1991). Thus, the abnormal LVs isolated from myo1a KO mice provide strong evidence indicating that these membranes are microvillus derived. The vesicles isolated from KO mice could be produced in one of two ways: (1) actively, by myosin motors that redistribute into the brush border in the absence of myo1a or (2) passively, perhaps via mechanical shearing of large membrane herniations from the apical surfaces of KO enterocytes (Tyska et al., 2005). This type of unregulated membrane loss could explain the increased variability observed in vesicle size (Fig. 4-6) and density (Fig. 4-7 A) as well as the increased amounts of proteins such as SI, LPH, and MGAM that are normally excluded from LVs and retained in the microvillar membrane (Fig. 4-7, B and C).

The precise role of myo1a-derived forces in the formation of LVs and their subsequent release from microvillar tips remains unclear. However, it is possible that mechanical forces exerted on the membrane along the microvillar axis may provide a physical stimulus that leads to the fission of membrane from microvillar tips (Hobbs, 1980). Alternatively, myo1a might play a role in the sorting of specific high curvature lipids or other fission machinery into the tip compartment, a possibility discussed in more detail in the following section. Elucidating the details of how myo1a contributes to the formation and release of LVs will likely become the focus of future studies.

Enrichment of IAP at the microvillus tip

Actin-based cellular protrusions have been shown to enrich transmembrane proteins at their distal tips to carry out specialized functions such as mechano-sensitive ion gating in the case of stereocilia (Hudspeth and Gillespie, 1994) or integrin-mediated cellular adhesion in the case of filopodia(Zhang et al., 2004). Although microvilli are a classical model for studying organized actin arrays (Mooseker and Tilney, 1975), little is known about the distribution of membrane or cytoskeletal components along the microvillar axis. The first protein to be localized to the microvillus tip was the actin-regulating protein Eps8 (Croce et al., 2004). Another recent study has shown that ezrin and the ezrin-interacting protein EPI64 localize in a gradient with highest levels at the microvillar tip (Hanono et al., 2006). To our knowledge, the IAP enrichment described in this study is the first demonstration of microvillus tip localization for a membrane protein.

An interesting question arises as to the mechanism that may drive the polarized localization of IAP. Transmembrane proteins that localize to the tips of stereocilia and filopodia are transported to the protrusion's distal end by myosin motor proteins (Delprat et al., 2005; Tokuo and Ikebe, 2004). However, because IAP is localized to the extracellular leaflet of the plasma membrane by a glycosylphosphatidylinositol linkage, it does not have direct access to motor proteins that might provide plus end–directed transport. Viewed from an alternate perspective, lack of tethering to the underlying cytoskeleton might be important for allowing the "flow" of IAP along the microvillar axis and into the tip

compartment; molecules that are tethered to the actin core may be prevented from flowing toward the distal tip. We postulate that tipward flow of untethered membrane components could be driven by the biosynthetic delivery of material to the base of microvilli and release of vesicles from microvillar tips. This hypothesis is consistent with a previous study, which established that SI, a type II transmembrane protein, interacts directly with myo1a and that this interaction is required to retain SI in the brush border (Tyska and Mooseker, 2004). This idea also finds support in the biochemical and immunofluorescence data presented in this study, which reveal that although LVs contain SI, levels are low compared with brush border membranes (Fig. 4-4). Moreover, in the absence of myo1a, SI levels in the brush border decrease, whereas more of this transmembrane protein is found in LVs (Fig. 4-7). In combination, these data support a model in which differential tethering to the actin core via motors such as myo1a plays an important role in producing the enrichment of specific components (e.g., IAP) at microvillar tips.

Mechanism of LV formation and release from microvillar tips

A key goal for future studies will be to investigate the mechanistic details of LV formation and release from microvillar tips as well as the regulation of this process by physiological and pathophysiological stimuli. Clues to the machinery involved in this process may be found in the LV proteome described in this study (Table I). FAVS-purified LVs contain several proteins that are expressed at high levels in the enterocyte brush border (Table I). Among these are several lipid-

binding proteins, including eight members of the annexin family (A1-5, A7, A11, and A13b) and secreted PLA2 (Table S1). These components are of particular interest because annexins are involved in mediating actin–membrane interactions (Hayes et al., 2004; Merrifield et al., 2001) during several membrane fission and fusion events (Gerke et al., 2005) and thus may play a key role in the formation or release of LVs from the actin-rich microvillus. PLA2 hydrolyzes phospholipids into arachidonic acid and lysophospholipids and thus plays a key role in the generation of proinflammatory second messengers such as prostaglandins and leukotrienes (Dennis et al., 1991). Because it removes the *sn*-2 acyl chain of phospholipids, PLA2 activity also changes membrane curvature, which has been shown to cause the spontaneous fission and vesiculation of lipid rafts from liposomes in vitro (Staneva et al., 2004). This is of particular interest, as both the microvillar membrane and LVs are enriched in proteins that preferentially partition into lipid rafts such as IAP.

Physiological function of microvillar membrane shedding

The release of vesicles laden with catalytically active hydrolases could allow processing of target substrates to take place without the need for substrate to be in direct contact with the enterocyte apical surface (Jacobs, 1983). Although previous ultrastructural studies described the presence of such vesicles in the intestinal lumen (DeSchryver-Kecskemeti et al., 1989; Halbhuber et al., 1994), the cellular origin of these vesicles remained unclear. Interestingly, compositional differences between vesicles and the enterocyte plasma membrane were originally interpreted as evidence that the vesicles were not derived from the

brush border (DeSchryver-Kecskemeti et al., 1989). However, the enrichment of specific enzymes at sites of vesicle release, such as IAP enrichment at microvillar tips (Fig. 4-4 E), would explain this apparent discrepancy.

The enrichment of IAP in LVs suggests that a primary function of these vesicles is the distribution of phosphatase activity throughout the intestinal lumen. Although the precise role of IAP in the gastrointestinal tract was unknown for many years, recent work in mouse and zebrafish model systems now shows that IAP is a vital component of the mucosal barrier (Bates et al., 2007; Beumer et al., 2003; Goldberg et al., 2008; Su et al., 2006; van Veen et al., 2005). Specifically, IAP is able to dephosphorylate and thus detoxify bacterial lipopolysaccharide (LPS). An abundant component of the gram-negative bacterial outer membrane, LPS is a potent and highly concentrated proinflammatory ligand in the gastrointestinal tract; dephosphorylation of the lipid A moiety of LPS reduces the toxicity of this compound at least 100-fold (Schromm et al., 1998). The production of IAP-enriched LVs could be a mechanism that enterocytes use to detoxify LPS in the intestinal lumen in an effort to minimize its proinflammatory impact on cells of the mucosa.

Concluding remarks

Microvillar membrane shedding represents a novel aspect of epithelial cell biology that may provide the enterocyte with a means for catalytically conditioning the lumenal environment. Given that LVs are specifically enriched in IAP activity, which may be involved in host defense against gram-negative bacteria, these vesicles may play an important role in mucosal barrier function. The work

presented in this study provides a critical first step toward understanding the role of this new aspect of enterocyte function. Future studies will attempt to illuminate the molecular mechanisms governing LV function and seek to identify physiological stimuli that may regulate LV release.

Table 4-1. Proteins identified in IAP-enriched LVs by shotgun mass spectrometry.

Accession Number	Coverage	Peptides	Protein
IPI:IPI00189819.1	41%	14	Actin
IPI:IPI00231966.5	11%	2	ADP-ribosylation factor 4
IPI:IPI00230862.7	44%	39	Aminopeptidase N
IPI:IPI00563187.2	74%	91	amylase 2
IPI:IPI00212767.1	13%	2	Anionic trypsin-1
IPI:IPI00231615.5	11%	3	Annexin A1
IPI:IPI00364621.2	20%	8	Annexin A11
IPI:IPI00366259.3	64%	22	annexin A13
IPI:IPI00325146.6	38%	12	Annexin A2
IPI:IPI00207390.9	13%	4	Annexin A3
IPI:IPI00231968.4	43%	16	Annexin A4
IPI:IPI00471889.7	10%	3	Annexin A5
IPI:IPI00361924.3	10%	5	Annexin A7
IPI:IPI00358059.2	24%	8	Aspartyl aminopeptidase
IPI:IPI00211548.1	59%	36	Bile salt-activated lipase
IPI:IPI00368397.2	56%	19	BWK3
IPI:IPI00392472.2	12%	13	calcium activated chloride channel 4
IPI:IPI00325435.3	12%	4	Calpain-5
IPI:IPI00327713.1	16%	5	Carboxypeptidase A1
IPI:IPI00211212.1	11%	2	Cationic trypsin-3
IPI:IPI00882402.1	8%	2	CD82 antigen
IPI:IPI00195627.1	42%	30	chloride channel calcium activated 3
IPI:IPI00417388.1	7%	4	Choline transporter-like protein 4
IPI:IPI00213599.1	40%	8	Chymotrypsin-C
IPI:IPI00206309.1	37%	10	Chymotrypsinogen B

Accession Number	Coverage	Peptides	Protein
IPI:IPI00360099.2	18%	2	Clarin-3
IPI:IPI00212799.1	46%	6	Colipase
IPI:IPI00480639.3	8%	10	Complement C3
IPI:IPI00193445.1	6%	2	Creatine kinase
IPI:IPI00208448.4	22%	10	CUB and zona pellucida-like domain-containing protein 1
IPI:IPI00471530.2	56%	23	Cytosol aminopeptidase
IPI:IPI00327697.4	45%	14	Dipeptidase 1
IPI:IPI00777229.1	18%	13	Dipeptidyl peptidase 4
IPI:IPI00326462.1	36%	27	Ectonucleotide pyrophosphatase/phosphodiesterase family member 3
IPI:IPI00324820.3	15%	3	EGP-314 protein homologue
IPI:IPI00365289.3	20%	4	elastase 3B, pancreatic
IPI:IPI00327729.1	12%	2	Elastase-1
IPI:IPI00212792.1	19%	5	Elastase-2A
IPI:IPI00192837.3	18%	8	EPS8-like 3
IPI:IPI00470254.4	6%	3	Ezrin
IPI:IPI00364948.3	26%	10	Fatty aldehyde dehydrogenase
IPI:IPI00206396.1	7%	3	Fatty-acid amide hydrolase 1
IPI:IPI00777061.1	44%	10	Ferritin heavy chain 1
IPI:IPI00211324.1	23%	8	Galectin-4
IPI:IPI00327398.1	39%	35	Glutamyl aminopeptidase
IPI:IPI00734632.2	23%	10	Granule glycoprotein GP2
IPI:IPI00209163.1	25%	3	histone 2, H2be
IPI:IPI00561052.3	26%	3	Histone H4
IPI:IPI00208205.1	6%	4	Hspa8
IPI:IPI00388764.1	35%	7	hypothetical protein LOC363490
IPI:IPI00769183.2	37%	7	hypothetical protein LOC691352
IPI:IPI00188967.1	85%	8	Ig kappa chain C region, A allele
IPI:IPI00389419.2	50%	19	Igha_mapped protein
IPI:IPI00196395.1	55%	30	Intestinal Alkaline Phosphatase (Akp3)
IPI:IPI00327516.3	54%	30	Intestinal alkaline phosphatase 1 (Alpi)
IPI:IPI00194045.1	9%	3	Isocitrate dehydrogenase [NADP] cytoplasmic
IPI:IPI00207014.2	10%	6	Keratin, type I cytoskeletal 19
IPI:IPI00764148.1	15%	27	Lactase-phlorizin hydrolase
IPI:IPI00197711.1	18%	6	L-lactate dehydrogenase A chain
IPI:IPI00361346.2	27%	13	LOC367586 protein
IPI:IPI00213231.5	19%	12	Long-chain-fatty-acid--CoA ligase 5

Accession Number	Coverage	Peptides	Protein
IPI:IPI00231381.7	31%	21	Major vault protein
IPI:IPI00193894.4	39%	59	Maltase-Glucoamylase
IPI:IPI00197684.1	28%	19	Membrane-bound aminopeptidase P
IPI:IPI00210872.5	9%	5	Meprin A subunit alpha
IPI:IPI00204808.5	21%	13	Meprin A subunit beta
IPI:IPI00551567.1	17%	2	MHC class I RT1-Au heavy chain (Fragment)
IPI:IPI00212316.1	8%	6	microsomal triglyceride transfer protein
IPI:IPI00200640.1	2%	2	Mucin and cadherin-like protein
IPI:IPI00208856.1	33%	21	Mucin-13
IPI:IPI00201262.1	7%	8	Mug2 Alpha-1-inhibitor 3
IPI:IPI00197154.1	31%	15	N-acetylated-alpha-linked acidic dipeptidase-like protein
IPI:IPI00231789.5	38%	28	Neprilysin
IPI:IPI00211648.1	11%	7	Neutral and basic amino acid transport protein rBAT
IPI:IPI00208165.1	13%	9	Neutral ceramidase
IPI:IPI00192495.3	7%	5	Nicastrin
IPI:IPI00212662.1	41%	16	Pancreatic lipase-related protein 1
IPI:IPI00231487.5	48%	19	pancreatic lipase-related protein 2
IPI:IPI00198916.1	58%	27	Pancreatic triacylglycerol lipase
IPI:IPI00192334.1	56%	9	Phospholipase A2
IPI:IPI00776761.1	10%	3	Phospholipid scramblase 1
IPI:IPI00193303.3	11%	2	placenta-specific 8
IPI:IPI00231197.6	11%	6	Platelet glycoprotein 4
IPI:IPI00205255.1	18%	16	Polymeric immunoglobulin receptor
IPI:IPI00361888.3	4%	3	Polyubiquitin
IPI:IPI00191748.3	25%	8	Proteasome subunit alpha type-1
IPI:IPI00476178.3	29%	7	Proteasome subunit alpha type-3
IPI:IPI00231046.8	17%	5	Proteasome subunit alpha type-4
IPI:IPI00191501.1	29%	8	Proteasome subunit alpha type-6
IPI:IPI00215243.3	37%	8	Proteasome subunit alpha type-7
IPI:IPI00198237.1	24%	6	Proteasome subunit beta type
IPI:IPI00191749.5	38%	9	Proteasome subunit beta type-1
IPI:IPI00188584.1	26%	6	Proteasome subunit beta type-2
IPI:IPI00191505.3	24%	5	Proteasome subunit beta type-4
IPI:IPI00196791.2	28%	6	Proteasome subunit beta type-8
IPI:IPI00196819.5	19%	5	Proteasome subunit beta type-9
IPI:IPI00198887.1	61%	35	Protein disulfide-isomerase
IPI:IPI00324741.2	43%	22	Protein disulfide-isomerase A3

Accession Number	Coverage	Peptides	Protein
IPI:IPI00197568.2	17%	7	Rab GDP dissociation inhibitor beta
IPI:IPI00370158.3	8%	2	RAS-related C3 botulinum substrate 2
IPI:IPI00779473.1	7%	2	Serpinb1a -elastase inhibitor A
IPI:IPI00191737.6	47%	29	Serum albumin
IPI:IPI00339124.2	22%	5	Sodium/potassium-transporting ATPase subunit beta-1
IPI:IPI00203360.1	3%	2	Solute carrier family 15 member 1
IPI:IPI00767004.1	14%	5	sphingomyelinase, intestinal alkaline
IPI:IPI00191437.4	38%	20	Sucrase Isomaltase
IPI:IPI00212367.1	22%	5	syncollin
IPI:IPI00200117.1	17%	3	Syntenin-1
IPI:IPI00199458.1	3%	1	Tetraspanin 1
IPI:IPI00195931.1	30%	8	Tetraspanin 8 (D6.1A protein)
IPI:IPI00231139.6	9%	5	transketolase
IPI:IPI00192796.3	5%	3	Transmembrane 9 superfamily protein member 3
IPI:IPI00366513.3	18%	7	trehalase
IPI:IPI00554004.1	5%	2	UDP glucuronosyltransferase 2
IPI:IPI00213569.1	12%	6	UDP-glucuronosyltransferase 1-1
IPI:IPI00201969.1	9%	3	Vesicle amine transport protein 1 homolog
IPI:IPI00421874.4	29%	6	Voltage-dependent anion-selective channel protein 1
IPI:IPI00198327.2	22%	6	Voltage-dependent anion-selective channel protein 2
IPI:IPI00194721.3	50%	6	Zymogen granule membrane protein 16
IPI:IPI00368643.2	25%	2	13 kDa protein
IPI:IPI00556944.2	34%	3	14 kDa protein
IPI:IPI00560461.1	24%	3	15 kDa protein
IPI:IPI00781546.1	25%	59	263 kDa protein
IPI:IPI00202725.1	20%	2	40S ribosomal protein S21
IPI:IPI00215107.3	12%	3	40S ribosomal protein SA

CHAPTER V

LUMENAL VESICLES PLAY A ROLE IN HOST DEFENSE

Introduction

The intestinal lumen is home to an astoundingly large (~10^{14}) and diverse microbial population (Backhed et al., 2005). From the host perspective, allowing this *microbiota* to survive can be advantageous as these organisms bring additional metabolic functionality to the lumenal environment. However, one challenge associated with this mutualistic relationship is that mucosal epithelial cells must co-exist in intimate contact with lumenal microbes without succumbing to the toxic compounds and metabolites that are normally associated with bacterial populations. One such compound that is present at high levels in the intestinal lumen is the gram-negative bacterial outer membrane component, lipopolysaccharide (LPS, also known as “endotoxin”). LPS is a potent pro-inflammatory compound released from microbes as a soluble factor during cell division, growth, and death (Magalhaes et al., 2007). In addition to having an immediate impact on mucosal epithelial cells, LPS that crosses the intestinal barrier can cause systemic complications including vascular collapse, coagulation, sepsis, and even death (Mayeux, 1997; Parrillo, 1993). LPS toxicity is particularly problematic in patients receiving total parenteral nutrition following surgery or trauma (Buchman et al., 1995; Hise et al., 2008; Lipman, 1995), as the

prolonged absence of enteral stimulation is believed to impair mucosal barrier function (Hermsen et al., 2009). How cells of the intestinal mucosa protect themselves and distal systemic tissues from harmful bacterial products such as LPS is a critical yet poorly understood aspect of gastrointestinal biology.

Combined with our studies demonstrating the realese of IAP-enriched lumenal vesicles (LVs) from microvillar tips (McConnell et al., 2009), these data suggest that LVs may play an important role in minimizing LPS toxicity in the gut.

Consistent with a role in host defense, microvillus-derived vesicles physically interact with lumenal bacteria, dephosphorylate purified bacterial lipopolysaccharide, protect cultured epithelial cells from the pro-inflammatory signaling normally stimulated by this microbial product, and are produced in response to feeding. Based on these new data, we propose that microvillar membrane shedding represents a novel mechanism for deploying host defense machinery throughout the intestinal lumen.

Results

LVs physically interact with lumenal bacteria

Recent studies have shown that IAP plays a critical role in protecting the mucosa from bacteria by dephosphorylating the toxic bacterial outer membrane component LPS (Bates et al., 2007; Goldberg et al., 2008; Koyama et al., 2002). Because LVs are enriched in IAP and exhibit robust phosphatase activity (McConnell et al., 2009), we sought to investigate the possibility that microvillar membrane shedding could play a role in mucosal defense against lumenal microbes, e.g. by distributing IAP activity throughout the lumen to detoxify

microbe-associated or soluble LPS. Consistent with this possibility, TEM analysis of negatively stained lumen wash samples revealed numerous bacteria that were coated with clusters of vesicles (Fig. 5-1 A). When material from lumen wash fractions was fluorescently labeled with DiD (to visualize LV lipids), anti-IAP, and DAPI (to visualize bacteria), confocal imaging confirmed that these clusters were composed of vesicles that were positive for IAP (Fig. 5-1 B and C). These images indicate that IAP-enriched LVs from our preparation are able to physically interact with native, lumenal microbes.

LVs dephosphorylate and detoxify bacterial LPS

To determine if LV-associated IAP is capable of chemically modifying LPS, we incubated LVs (25 μg total protein) with a series of LPS concentrations and measured phosphate release using a malachite green assay (Baykov et al., 1988). To compare the activity of LVs with the activity found at the mucosal surface, we also incubated LPS with brush borders (25 μg total protein) isolated from the same animals used for LV preparations. These assays revealed robust LPS-dependent phosphate release in both the LV and brush border reactions. Moreover, in both cases phosphate release was inhibited by 10 mM L-phenylalanine (Fig. 5-2 A), an inhibitor specific to intestinal-type alkaline phosphatase (Fernley and Walker, 1970).

Given that dephosphorylation of LPS significantly reduces the toxicity of this compound by interfering with its ability to activate pro-inflammatory signaling in target cells (Poelstra et al., 1997), we examined the toxicity of LV-"conditioned" LPS. Phosphorylated LPS induces an inflammatory response by activating the

Nuclear Factor kappa B (NF-kB) transcription pathway in a concentration-dependent manner (Kojima et al., 2004). Thus, we assayed LPS toxicity by measuring the extent of NF-kB phosphorylation induced in cultured epithelial cells following LPS exposure (Fig. 5-2 C). For this experiment, LPS was incubated overnight with or without LVs isolated from *ad libitum* fed mice; LVs were removed by centrifugation prior to applying the samples to cells. Strikingly, LVs were able to completely eliminate the pro-inflammatory effects of LPS relative to controls, with no apparent increase in NF-kB phosphorylation, even at LPS concentrations up to 10 μg/mL (Fig. 5-2 C). In combination, data from these biochemical and cell culture assays demonstrate that LV-associated IAP activity is able to dephosphorylate and thus detoxify bacterial LPS.

LV production and lumenal capacity for detoxifying LPS are regulated by feeding

Previous studies have established that mucosal IAP expression is regulated by access to nutrition; expression is reduced during starvation and increases in response to feeding (Hodin et al., 1994). Normal enteral feeding has been shown to have important positive effects on the integrity of the intestinal mucosa, whereas total parenteral nutrition, which is often used to sustain critically ill patients, can result in intestinal inflammation and reduced barrier function (Hise et al., 2008). Thus, we sought to determine if access to nutrition also regulated the production of IAP-enriched LVs. For this experiment, we first examined the impact of fasting on the steady–state level of LVs in the lumen. Lumen wash samples from *ad libitum* fed mice or animals fasted for 16 hours were processed

stoichiometrically (e.g. flushed with equal volumes) and the LV fraction was prepared as described above. Visual inspection revealed that preparations from fasted animals yielded substantially smaller 100,000 *x g* LV pellets (Fig. 5-2 B). Protein assay of the 100,000 *x g* LV pellets confirmed that fasted mice harbor reduced levels of LV material at steady-state ($p < 0.01$). Strikingly, fasted LV samples also showed significantly lower IAP signal on a Western blot and dramatically reduced IAP activity ($p < 0.01$, Fig. 5-2 B). In light of these findings, we reasoned that the lumenal capacity for detoxifying LPS would also be compromised in fasted animals. Indeed, when compared to the detoxifying activity of samples from *ad libitum* fed mice, LVs isolated from fasted mice only modestly decreased NF-κB phosphorylation in the cell culture toxicity assay described above (Fig. 5-2 C). These studies clearly show that enteral nutrition regulates the production of IAP-enriched LVs and thus, the LPS-detoxifying capacity of the intestinal lumen.

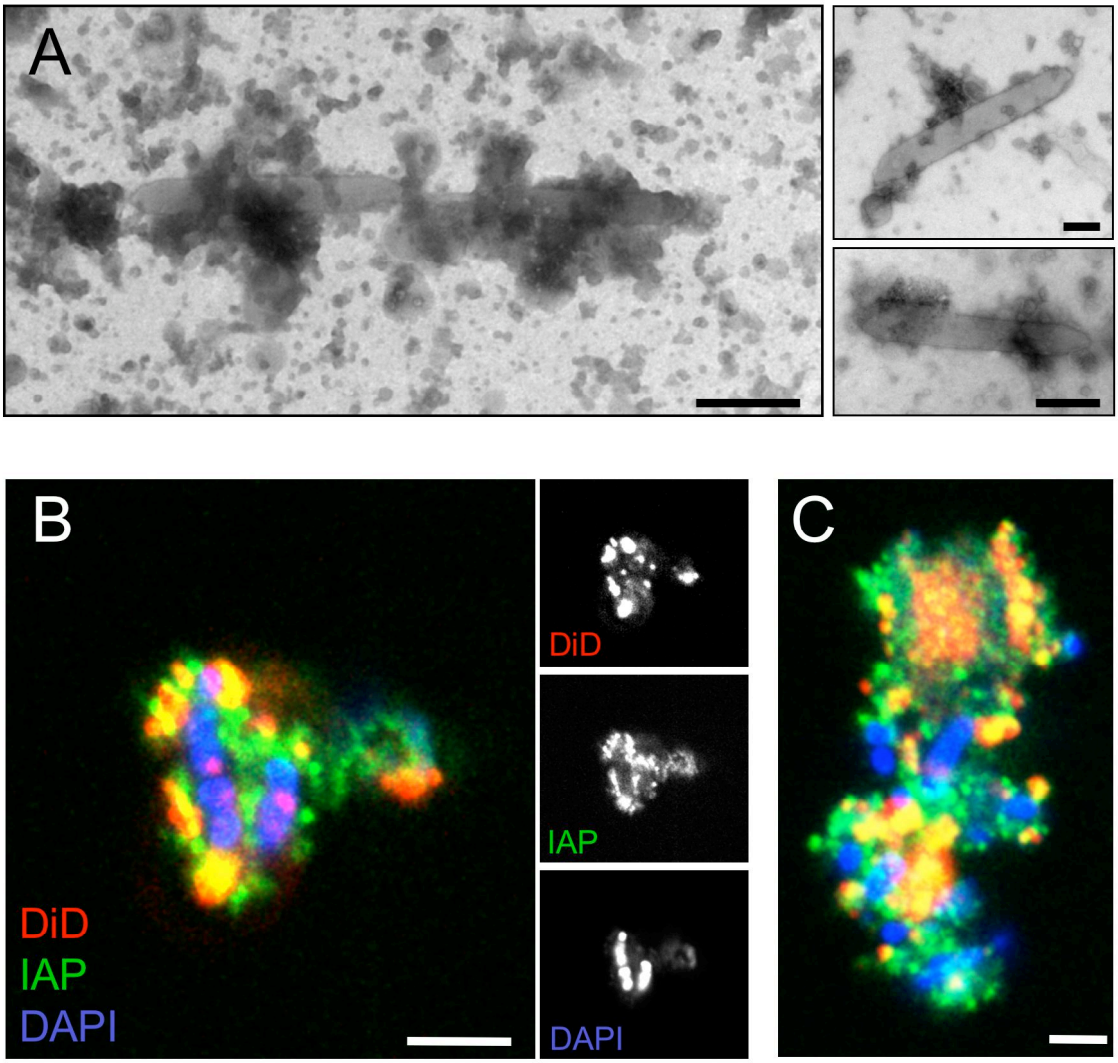

Figure 5-1. IAP-positive LVs interact with native lumenal bacteria.
(A) Negative stain TEM shows clusters of LVs around native bacteria (large rods). Bars = 0.2 μm. **(B-C)** Confocal micrographs show that LVs interacting with lumenal bacteria are positive for IAP. LVs were labeled with an anti-IAP antibody (green) and the lipophilic dye DiI (red); bacteria were visualized with the DNA dye DAPI (blue). Bars = 2 μm.

Summary

The experiments described here clearly demonstrate that native LVs are capable of dephosphorylating LPS and protecting epithelial cells from the pro-inflammatory signaling normally induced by this compound. In addition, the production of IAP-enriched LVs and their associated capacity for detoxifying LPS are regulated by feeding. This is consistent with data showing that IAP expression and activity in the gut are decreased during fasting and restored upon refeeding (Goldberg et al., 2008; Hodin et al., 1994). The ability to reduce LPS toxicity by distributing IAP-enriched LVs may allow enterocytes to "tolerate" the indigenous gram-negative microflora that reside in the lumen; upregulation during feeding would allow the mucosa to compensate for the increased bacterial load that accompanies the influx of nutrients during this period. Indeed, oral administration of purified calf IAP was shown to attenuate LPS toxicity in mice and piglets, suggesting that high lumenal concentrations of IAP are in fact beneficial (Beumer et al., 2003). Constitutive detoxification of LPS may be even more important in cases where gut-derived LPS leaks through the mucosal barrier and enters the systemic circulation. Once outside the gut, LPS can exert powerful detrimental effects on a variety of organ systems; gut-derived LPS can exacerbate several forms of liver disease, contribute to chronic heart failure, stimulate vascular collapse, cause blood coagulation, lead to sepsis and even death (Caradonna et al., 2000). Thus, the release of IAP-enriched LVs from enterocyte microvilli represents a previously uncharacterized pathway for

distributing IAP activity into the intestinal lumen, and may be critical for protecting GI and non-GI organ systems from the detrimental effects of bacterial LPS.

Given that enterocyte microvilli are physically situated at the cellular interface with the lumenal environment, microvillar membrane shedding is ideally positioned to participate in the regulation of microbial-epithelial interactions. In addition to the enzymatic conditioning of the lumenal environment discussed above, LVs could contribute to mucosal barrier function in a much more direct fashion by limiting bacterial access to the mucosal surface, functioning in a manner similar to anti-microbial lectins (Cash et al., 2006).

LVs released from microvillar tips could serve as “decoys” for microbial binding in the lumen; these vesicles would serve to “soak up” bacteria or bacterial agents that would otherwise target the epithelial cell apical surface. The formation of LV-microbe complexes would restrict targeted bacteria to the lumen and inhibit further physical interactions with the mucosa. Our confocal imaging of LVs from native lumen wash preparations provides strong support for this hypothesis by showing that IAP-positive LVs cluster on the surface of native lumenal microbes.

The ability to physically interact with lumenal microbes becomes even more important in the context of virulent bacteria that rely on mucosal adherence for survival. The intestinal mucosa is a target of several common virulent bacterial species such as Salmonella typhimurium, Listeria monocytogenes, and a variety of pathogenic classes of Escherichia coli including Adherent and Invasive (AIEC), Enteropathogenic (EPEC), and Enterohemmorhagic (EHEC).

The first step in the pathogenesis of these microbes is physical adherence to the mucosal surface; adherence enables micro-colony formation and enhances microbial survival. Constitutive microvillar membrane shedding may represent a simple host defense mechanism that interferes with bacterial adherence and prevents colony formation on the enterocyte apical surface.

Microvillar membrane shedding represents a novel aspect of epithelial cell biology that provides the enterocyte with a means for “conditioning” the lumenal environment. In addition to its role in detoxifying lumenal lipopolysaccharide, the release of vesicles from microvillar tips may allow enterocytes to interfere with pathogenic bacterial-epithelial interactions. The work presented here provides a critical first step toward understanding the role of this new aspect of enterocyte biology and its contribution to mucosal barrier function and GI homeostasis. Future studies will attempt to illuminate the molecular mechanisms governing LV function and seek to identify the cellular mechanisms regulating LV release.

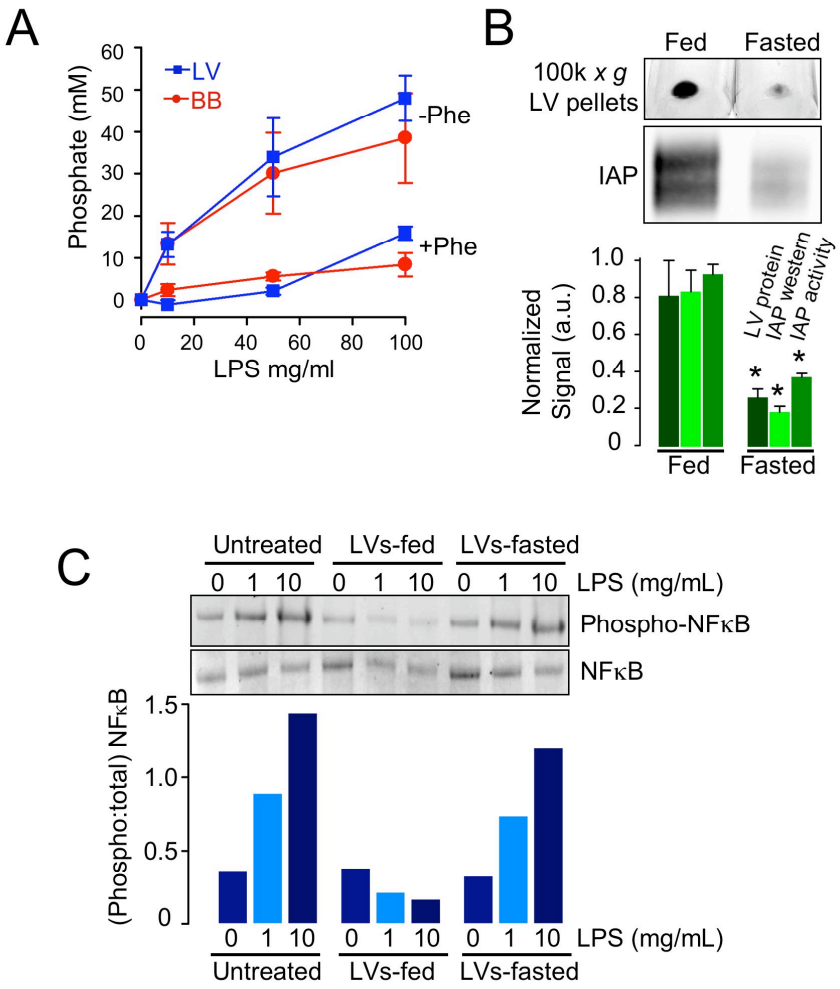

Figure 5-2. Fasting reduces LV production and the LPS detoxifying capacity of the intestinal lumen.

(A) LVs (blue squares) and isolated brush borders (red circles) were incubated with increasing concentrations of LPS and incubated at 37°C for 30 min. Samples were then taken from each reaction and the amount of phosphate released was determined using a malachite green assay. LVs and brush borders demonstrated similar phosphatase activities; furthermore, LV and brush border phosphatase activity was severely inhibited when incubated with 10mM L-Phe, an IAP inhibitor. **(B)** Pictures of the 100,000 *x g* pellets isolated from fed or fasted mice (16 hour fast) reveal that fasted mice released less material into the ultra-speed pellet than fed controls. Western blot analysis revealed a decrease in IAP protein, with a corresponding decrease in IAP activity (asterisks, $p < 0.01$), suggesting that the overall dephosphorylating capacity present in the fasted intestinal lumen was reduced relative to fed controls. **(C)** LPS was incubated at 37°C for 16 hrs either untreated, with 1 μg of LVs isolated from control mice, or LVs isolated from fasted mice (loaded stoichiometrically). All samples were centrifuged (100,000 *x g*) to remove LVs, the supernatants added to wells of confluent monolayers of LLC-PK1 epithelial cells, incubated at 37°C and 5% CO_2 for 5 minutes, and cells were then lysed in equal volumes of boiling sample buffer. Pro-inflammatory signaling induced by each sample was assessed by Western blot analysis of NF-kB phosphorylation. Bands were quantified by densitometry and the ratio of phosphorylated to total NF-kB was used as a measure of NF-kB signaling. LPS produced a robust, concentration-dependent increase in NF-kB signaling. LVs from fed mice were able to completely prevent NF-kB pathway activation; however, LVs from fasted mice were able to only modestly decrease NF-kB phosphorylation, suggesting an overall decrease in the LPS detoxifying capacity in the fasted relative to the fed gut.

CHAPTER VI

CONCLUDING REMARKS

The studies presented here describe a number of new discoveries. The first is that the microvillar actin bundle can be used by myosins as a track for directed movement. Although it has been known for almost four decades that the actin bundles in the microvillus are uniformly polarized (Mooseker and Tilney, 1975; Tilney and Mooseker, 1971), only recently have a handful of proteins that display polarized distributions along the microvillar axis been found (Croce et al., 2004; Hanono et al., 2006). The ability of motors to move directionally along these bundles suggests that more proteins, particularly those in the apical membrane, may be differentially localized via attachment to specific myosins. The findings presented in Chapter IV show that while IAP is preferentially localized to the microvillus tip, the myosin-1a interacting protein SI localizes along the length of the microvillus. This suggests that myosin-1a may anchor specific substrates along the length of the microvillus, excluding them from the microvillar tip. In agreement with this hypothesis, recent data from our laboratory has found that myosin-1a preferentially localizes along the length of microvilli, but is notably absent from the microvillus tip (Benesh et al., 2010).

Perhaps the most exciting finding of these studies is the discovery of a novel form of vesicle release from the tips of microvilli. In the gut, LVs appear to play a role in host defense by detoxifying the bacterial compound LPS (Chapter V). The presence of small vesicles in the lumens of other organs (kidney, liver,

brain) suggests that microvillar vesicle release may be a conserved function of all epithelia. What function(s) lumenal vesicles might mediate in these organ systems remains an open question, offering opportunities for future investigations.